Arc Phenomena and Gasdynamic Effects due to Interaction of Shock Waves with Magnetic Fields

H. Klingenberg

IPP 3/78 August 1968

INSTITUT FÜR PLASMAPHYSIK
GARCHING BEI MÜNCHEN

INSTITUT FÜR PLASMAPHYSIK

GARCHING BEI MÜNCHEN

Arc Phenomena and Gasdynamic Effects due to Interaction of Shock Waves with Magnetic Fields

H. Klingenberg

IPP 3/78 August 1968

Die nachstehende Arbeit wurde im Rahmen des Vertrages zwischen dem Institut für Plasmaphysik GmbH und der Europäischen Atomgemeinschaft über die Zusammenarbeit auf dem Gebiete der Plasmaphysik durchgeführt.

Index

ABSTRACT Page

1. INTRODUCTION 1

2. SHOCK TUBE DEVICE AND MAGNETIC FIELD SYSTEM 2

2.1 Shock tube 2
2.2 Measuring chamber 2
2.3 Electrodes 2
2.4 Short-circuiting bridges 2
2.5 Magnetic field 6

3. MEASURING APPARATUS 10

3.1 Rogowski coils 10
3.2 $v \cdot B \cdot d$ measuring setup 12
3.3 Multiplier, image converter, drum camera 12

4. MEASURING RESULTS AND DISCUSSION 14

4.1 Measuring procedure 14
4.2 Oscillograms and image converter pictures 14
4.3 Results of $v \cdot B \cdot d$ measurements 21
4.4 Results of current measurements 21
4.4.1 Evaluation method 21
4.4.2 Measuring results 22
4.4.3 Arc spots 25
4.5 Internal resistance of the current channel 27
4.5.1: One electrode pair 27
4.5.2: 5 electrode pairs 27
4.5.3: 25 electrode pairs 29
4.6 Discussion of the results 30
4.7 Calculation of the retarding force $\vec{j} \times \vec{B}_0 \cdot L$ 31
4.8 Results of the drum camera measurements 32
4.8.1 Streak pictures 32
4.8.2 Velocity of the observed fronts 35
4.9 Results of the multiplier measurements 35
4.10 Discussion of the drum camera and multiplier measurements 40

5. CONCLUDING REMARKS 41

REFERENCES 42

IPP 3/78 H. Klingenberg

Arc Phenomena and Gasdynamic Effects due to Interaction of Shock Waves with Magnetic Fields.

August 1968

ABSTRACT

The arc phenomena occurring on interaction of shock-heated plasma with a magnetic field were studied in order to achieve an approximately uniform current distribution in a certain volume using a number of small electrodes. This is necessary for producing plane gasdynamic effects such as reflected shocks and one-dimensional flow behind them in order to compare experimental results with theory.

The current amplitude depends on the surface area and the number of electrodes. It is governed by the complex boundary conditions in the plasma-to-electrode transition, which consists of narrow current channels leading to arc spots. The properties observed agree with those of normal arcs described in the literature. Owing to the complexity of the phenomena it is not possible to explain the results quantitatively. They can, however, be explained qualitatively by comparing them with those described in the literature on normal arcs.

The real aim to fill an interaction volume with current as uniformly as possible seems to have been achieved. Image converter pictures show a rather homogeneous incandescence in the interaction region.

The retarding force per unit area $\vec{j} \times \vec{B} \cdot L$ acting on the supersonic plasma flow is of the order of the total hydrodynamic pressure of the flow. Streak photographs show that the flow is slowed down, and reflected fronts are observed. Strictly speaking these are not shock fronts, but they can be interpreted as the plasma fronts that follow shock fronts in case of relaxation. At lower initial pressure, for instante at 0.5 torr, the reflected front is again reflected at the contact front.

Further work will have to be done to compare these results with theory.

1. INTRODUCTION

Since many plasma experiments involve complicated interactions between shock waves and magnetic fields, it is interesting to study such phenomena under simple conditions. A suitable example is provided by plane shock waves with a perpendicular magnetic field. At high shock Mach numbers, a plasma streaming with supersonic velocity $\vec{v}$ (with respect to the local velocity of sound), is produced behind the front. If the streaming plasma is now acted on by a transverse magnetic field $\vec{B}$, the charge carriers are subjected to $\vec{v} \times \vec{B}$ forces. Currents of density $\vec{j}$ can then flow through electrodes flush mounted on the inside of the shock tube and connected on the outside. The plasma is therefore subjected to retarding $\vec{j} \times \vec{B}$ forces directed opposite to the velocity $\vec{v}$ and is slowed down. Strong reduction of the plasma velocity results in secondary gasdynamic effects, such as reflected shock waves.

Theoretical treatment even of one-dimensional flow entails considerable mathematical difficulties since the interaction process is described by a system of coupled, non-linear, partial differential equations. Theoretical studies have therefore been restricted so far to one-dimensional flow with transverse magnetic field and uniform current perpendicular to the field and the flow. Plane secondary fronts are thus obtained as solutions.

The most comprehensive theoretical investigations of this kind were conducted by E. Rebhan /1/. This author studied the final, asymptotic, steady state of ideal gases outside the interaction region. Recently, M.R. Johnson /2/ investigated the steady and unsteady states of an ideal gas in the interaction region. Both of these authors find that when the interaction is sufficiently strong there should be a reflected plane shock wave and rarefaction waves, the latter modifying the intensity of the primary shock front. According to Rebhan a contact front may also occur.

Experiments allowing comparison with theoretical results thus have to satisfy (approximately at least) such simple conditions as one-dimensional flow, transverse magnetic field, and uniform, transverse current, the latter condition being difficult to meet.

All known experimental investigations have been conducted on shock tubes because this is an easy way to produce one-dimensional flow. In these experiments, electrodes of large surface area are flush mounted along the inside of the tube and connected on the outside. Many investigations of this type have been conducted by, for example, Pain and co-workers /3/. Like all other authors, Pain assumes that the current comes from the entire electrode surface and uniformly fills the interaction region.

Reflected luminous fronts have also been observed by means of streak pictures.

The results of the first interaction experiments conducted in our laboratory /4/ on a diaphragm shock tube fitted with single pairs of electrodes of large surface area showed, however, that the current flows in the form of arcs which may strike the electrodes at different points from one shot to the next. Arcs can be expected because the electrodes are cold and the currents are much higher than 10 A. A number of arc spots can already be observed on the electrodes after one shot. The current density distribution is then governed by the complicated boundary conditions prevailing in the narrow current channels in front of the electrode spots. It is certainly not uniform. The assumption of uniform current density distribution that has been made by various authors is therefore not satisfied. Comparison of their results with the theory is not possible. The luminous fronts that they have observed in streak pictures and interpreted as shock fronts need not be associated with one-dimensional flow.

The purpose of the investigations described here is to achieve experimentally a uniform current distribution (approximately at least) in order to fulfill the conditions of the theory and to produce plane gasdynamic effects associated with one-dimensional flow. Using heated electrodes capable of providing the required high current densities of several hundred amperes per square centimetre would entail very difficult technological problems. The arc phenomenon was therefore utilized by mounting many electrodes of small surface area alongside and behind one another and short-circuiting the pairs separately in an attempt to produce many arcs alongside and behind

one another in order to achieve a good approximation of the required uniform current distribution in the interaction volume. The interaction effects occurring for this current distribution were investigated by optical methods. Some of the results have already been published in another paper /5/.

2. SHOCK TUBE DEVICE AND MAGNETIC FIELD SYSTEM

2.1 Shock tube

The shock tube (inner diameter 10 cm, length approx. 13 m) is of the diaphragm type, cf. /6/. The driving gas is hydrogen (100 atm.), and the test gas is argon (e.g. 1 torr). For p_o = 1 torr, the shock Mach number at the measuring site (9 m from the diaphragm region) is then M_s = 11.8, the equilibrium temperature behind the shock front 10^4 °K, the flow velocity of the plasma 3 mm/μsec, and the conductivity 40 mhos, cf. /4/.

2.2 Measuring chamber

The measuring chamber has a square internal cross section (7 x 7 cm^2). A well-known method using a sharp cutter /7/ is used to cut out the rectangular flow from the circular flow of the shock tube. The measuring chamber is made of plexiglass and, owing to the danger of breakage, it is constructed in sections, these being sealed with O-rings and secured between tie plates. Figure 1 shows the measuring chamber with the cutter, tie plates, sections, small electrode pairs, short-circuiting bridges, and magnetic field coils. Figure 2 shows a section of the measuring chamber that includes five electrode pairs and windows for differential interferometer measurements, cf. /8/. The shadows appearing in the image converter photographs shown below are caused by the window frames, see Fig. 10 in Section 4.2.

2.3 Electrodes

Various sizes and numbers of electrodes were used. In order to provide a comparison with previous measurements /4/, a few measurements were made with one electrode pair having a surface area of 3 x 7 cm^2 (3 cm in the flow direction). These electrodes projected slightly from the wall, and so they were tapered in both directions, cf. /4/. Most of the measurements, however, were made with small electrodes 4.5 mm in diameter (see Figs. 1 and 2), first with one pair, then with five pairs transverse to the flow direction and five pairs in the flow direction, and finally with 25 pairs. For simplicity, the electrode configurations used are denoted by symbols, which are explained in Fig. 3.

2.4 Short-circuiting bridges

Each electrode pair was short-circuited separately with a copper bridge. When several electrode pairs were used, the bridges were of various lengths, as shown in Figs. 1 and 2. The total external DC resistance (bridges + electrodes) therefore varied between 1.1 and 1.6 mΩ. It was determined by a current-voltage measuring method, cf. /4/. The corresponding AC resistance was calculated, and it varied between 2.7 and 4 mΩ. The total inductance of each discharge circuit was measured with an inductance meter. For this purpose, the bridge was shorted between the electrodes with a wire, cf. /4/. The inductance varied between 0.3 and 0.55 μHy. The values 3 mΩ and 0.4 μHy can be taken as the mean values for resistance and inductance respectively.

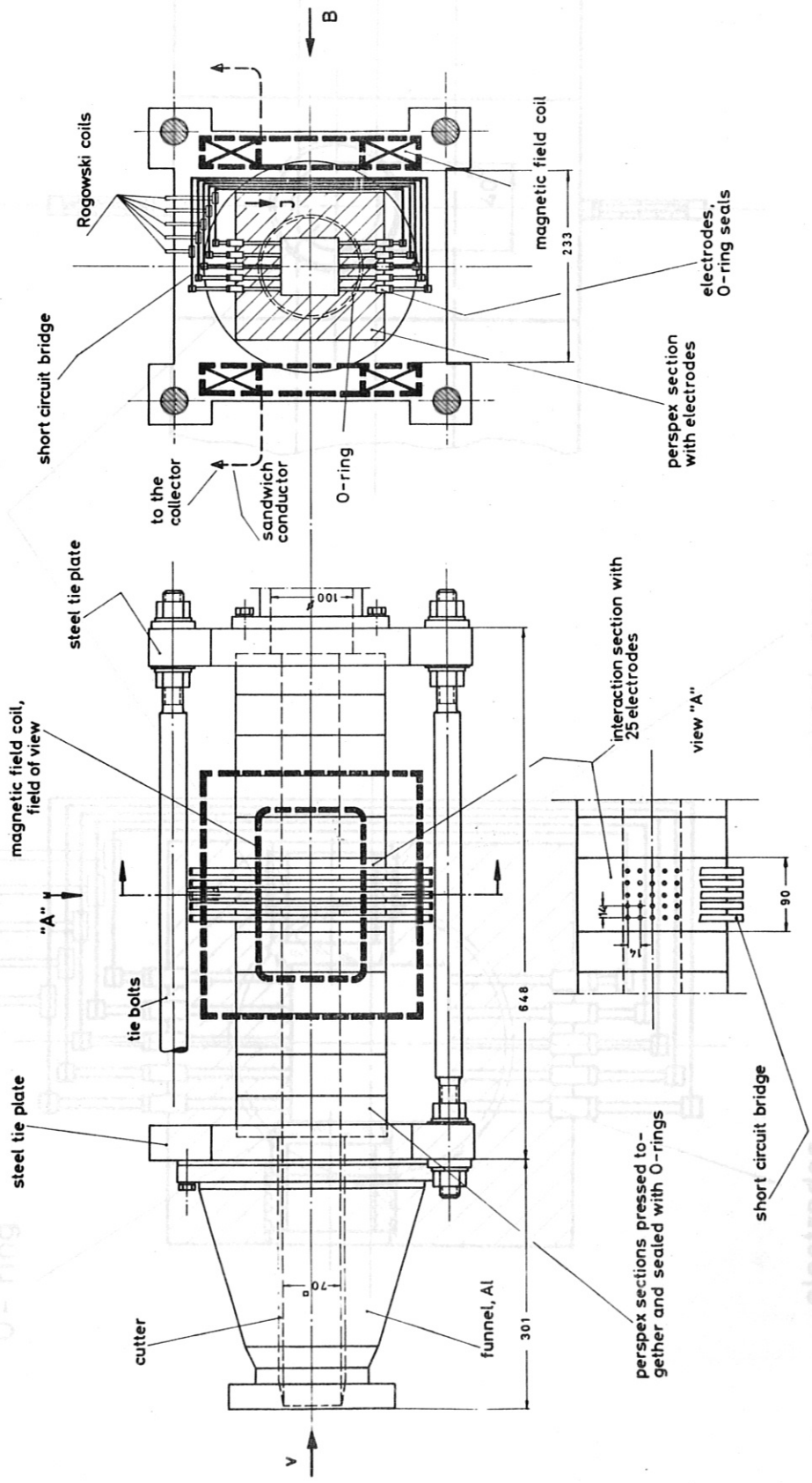

Fig. 1 Measuring chamber

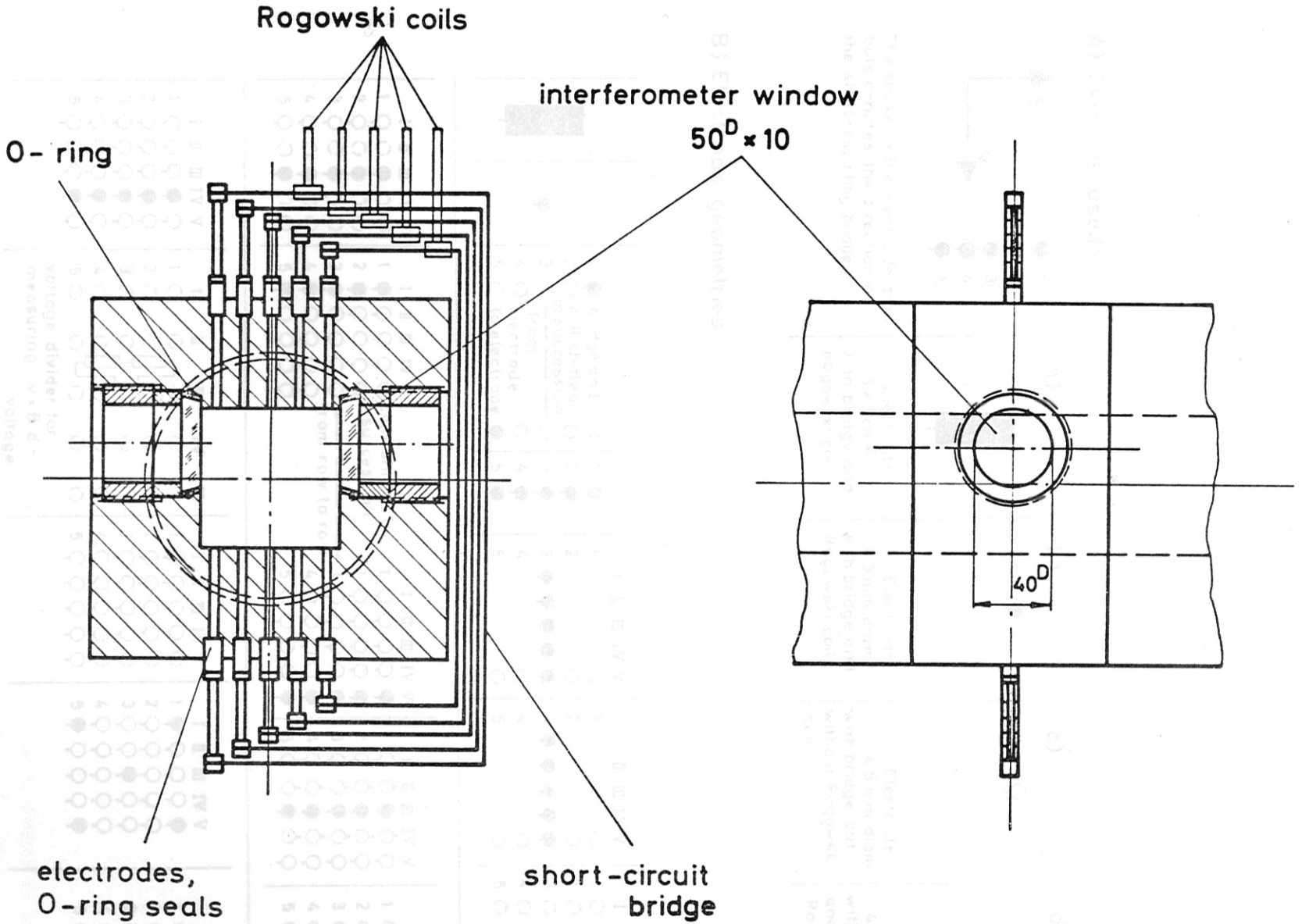

Fig. 2 Section with electrodes
and interferometer window

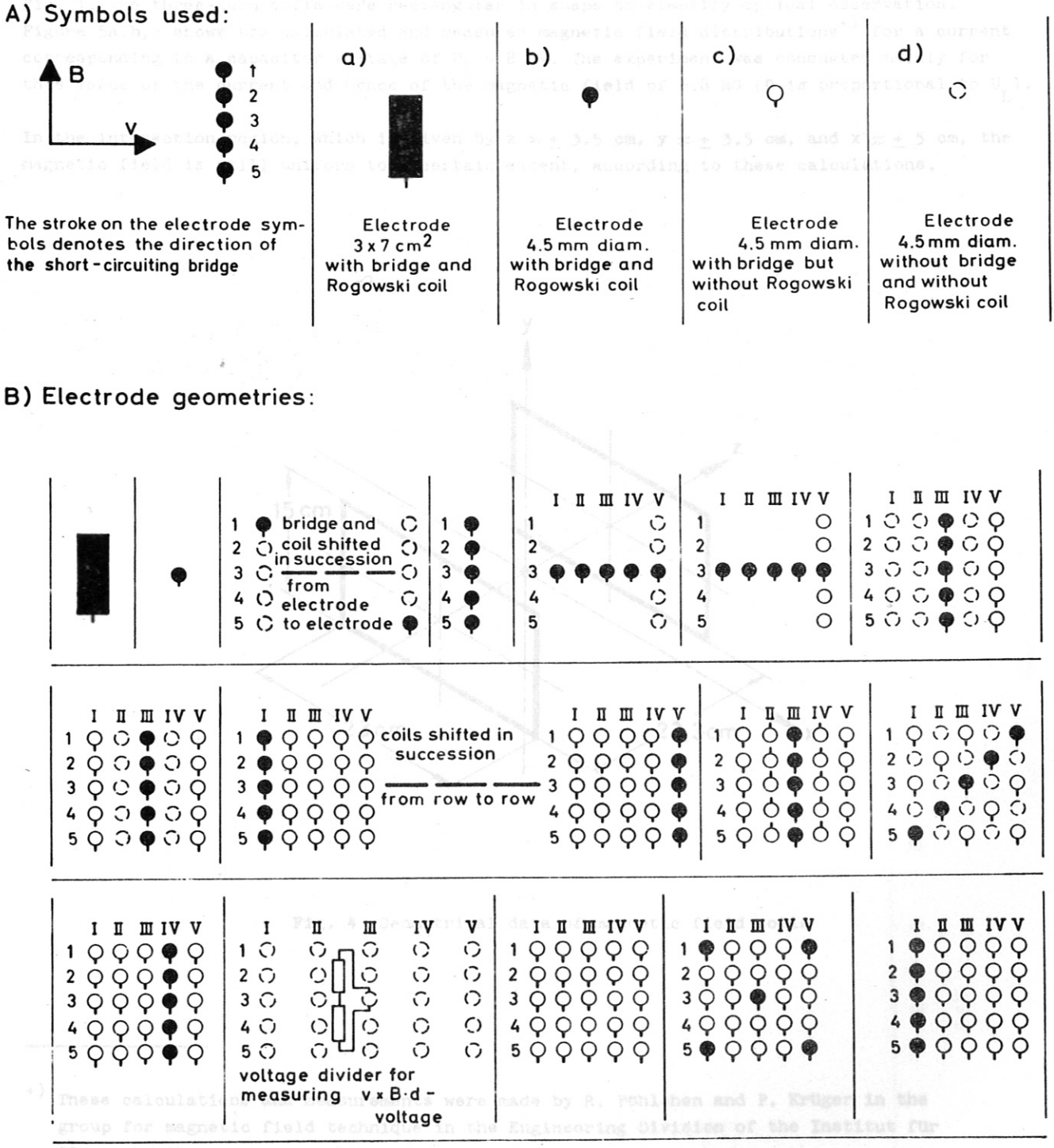

Fig. 3 Symbols, electrode geometries with direction of bridges

2.5 Magnetic field

The magnetic field was produced with a crowbarred capacitor bank (10 kV, 30 kJ) via coils similar to the Helmholtz type. The time constant $\tau = L/R$ for the crowbar discharge was raised relative to the previous experiment /4/, and so the magnetic field was more constant during the interaction period. Figure 4 shows the geometrical data of the magnetic field coils, see also Fig. 1. The three-turn coils were rectangular in shape to simplify optical observation. Figure 5a,b,c shows the calculated and measured magnetic field distributions[+)] for a current corresponding to a capacitor voltage of U_L = 8 kV. The experiment was conducted mainly for this value of the current and hence of the magnetic field of 6.8 kG (B is proportional to U_L).

In the interaction region, which is given by $z \approx \pm 3.5$ cm, $y \approx \pm 3.5$ cm, and $x \approx \pm 5$ cm, the magnetic field is still uniform to a certain extent, according to these calculations.

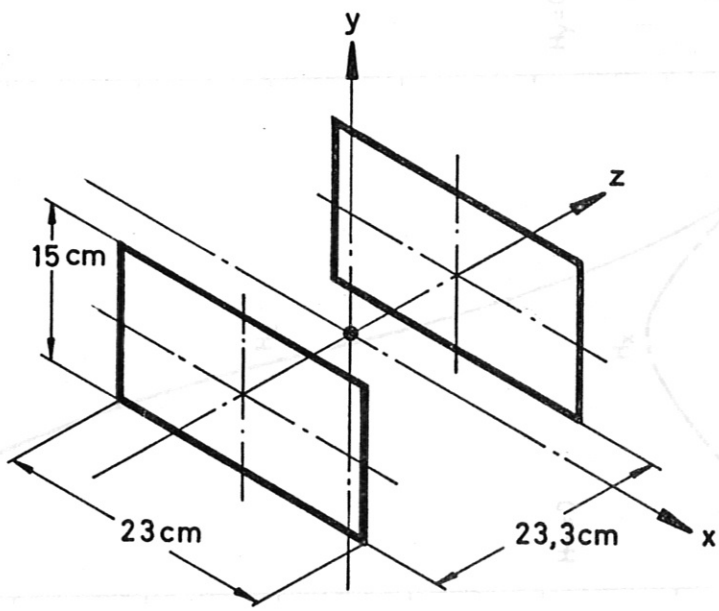

Fig. 4 Geometrical data of magnetic field coils

+) These calculations and measurements were made by R. Pöhlchen and P. Krüger in the group for magnetic field technique in the Engineering Division of the Institut für Plasmaphysik.

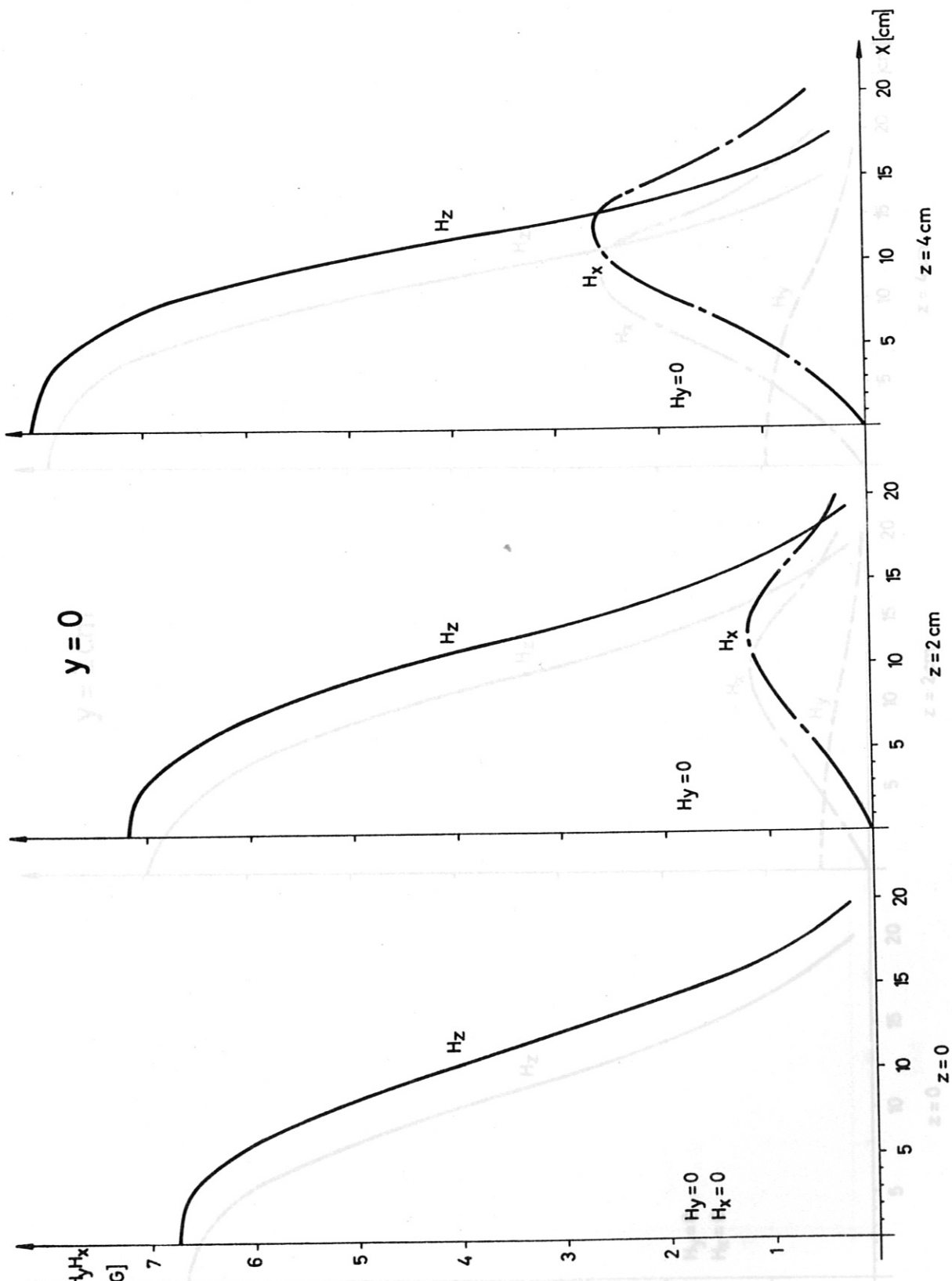

Fig. 5 a Magnetic field distribution

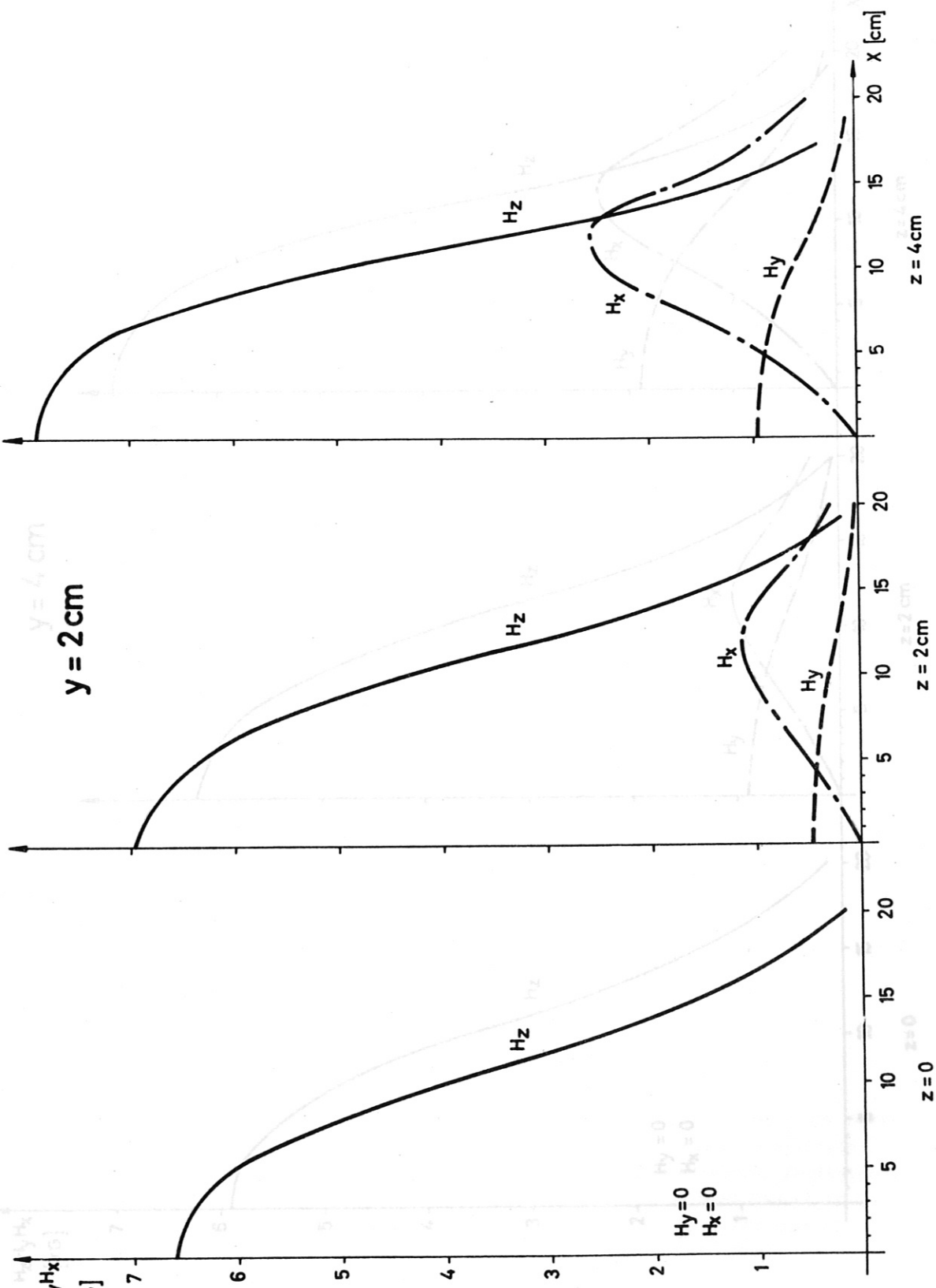

Fig. 5 b Magnetic field distribution

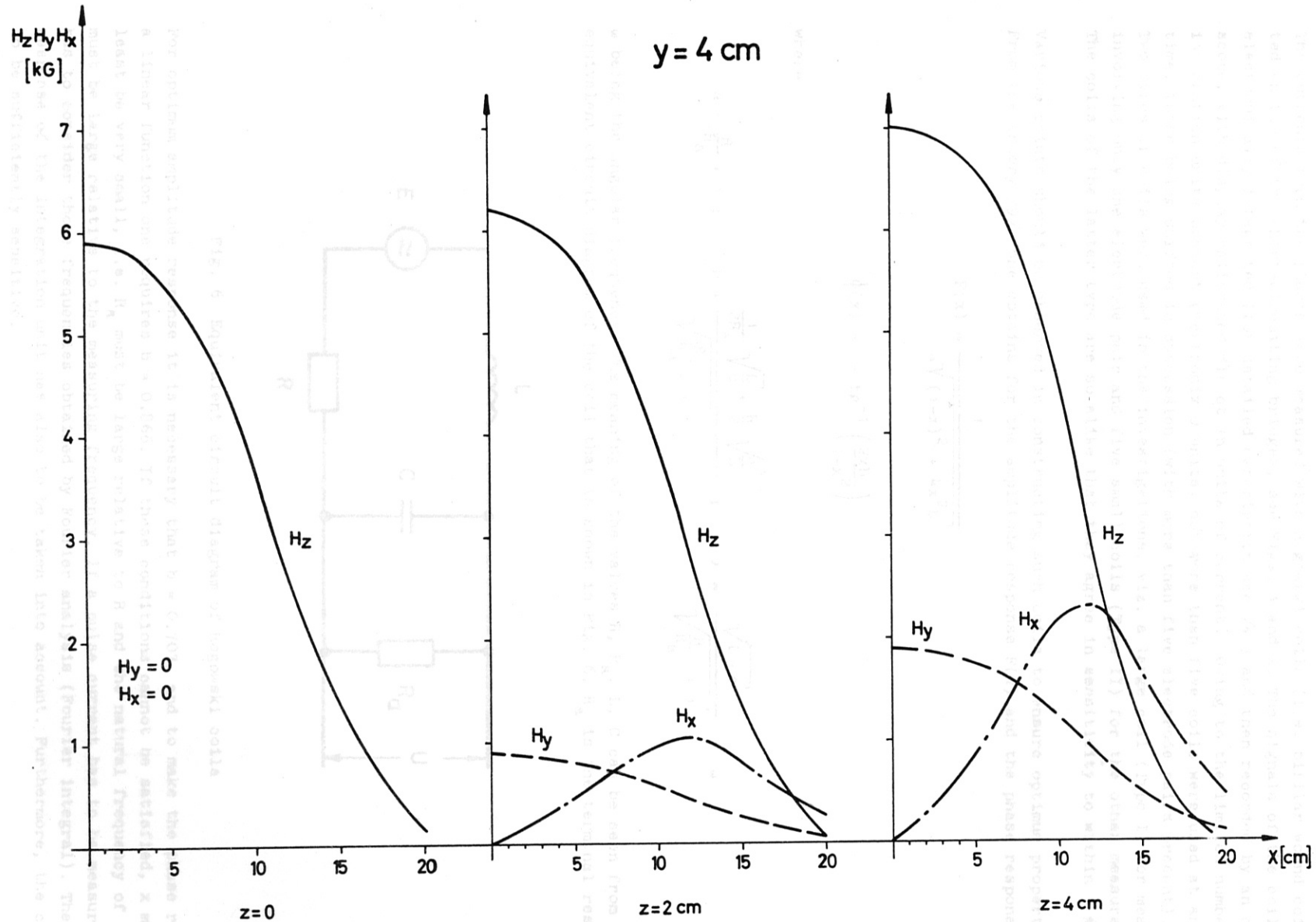

Fig. 5 c Magnetic field distribution

3. MEASURING APPARATUS

3.1 Rogowski coils

The currents from the plasma were measured with Rogowski coils (i.e. bifilar wound coils) mounted on top of the short-circuiting bridges, see Figs. 1 and 2. The signals of the coils were electronically integrated (for detailed description see /4/) and then recorded by an oscilloscope, with display calibrated direct in units of current. Owing to the limited number of integration units present (Tektronix O units) not more than five coils were used at any one time, these being shifted in succession (with more than five electrode pairs present).
Two types of coils were used in the investigations, viz. a large coil (Type I) for measurements involving only one electrode pair and five small coils (Type II) for the other measurements. The coils of the latter type are so alike that they agree in sensitivity to within 3 %.

Various points should be observed in constructing such coils to ensure optimum properties. From the theory /9/ one obtains for the amplitude response F(x) and the phase response $\phi(x)$:

$$F(x) = \frac{1}{\alpha\sqrt{(1-x)^2 + 4x^2 b}}$$

$$\phi(x) = - tg^{-1}\left(\frac{2xb}{1-x^2}\right)$$

where

$$\alpha = \frac{R}{R_a} + 1 \; ; \qquad b = \frac{\frac{1}{2R_a}\sqrt{\frac{L}{c}} + \frac{R}{2}\sqrt{\frac{c}{L}}}{\sqrt{\frac{R}{R_a} + 1}} \; ; \qquad x = \frac{\sqrt{L \cdot c}}{\sqrt{\frac{R}{R_a} + 1}} \cdot \omega$$

ω being the angular frequency. The meaning of the values R, R_a, L, C can be seen from the equivalent circuit diagram of the coil that is shown in Fig. 6. R_a is the terminal resistance.

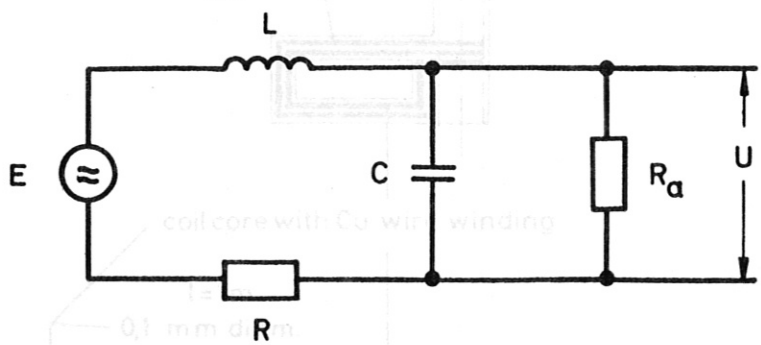

Fig. 6 Equivalent circuit diagram of Rogowski coils

For optimum amplitude response it is necessary that b = 0.707, and to make the phase response a linear function one requires b = 0.866. If these conditions cannot be satisfied, x must at least be very small, i.e. R_a must be large relative to R and the natural frequency of the coil must be large relative to the measuring frequency. If a pulse current has to be measured, one has to consider those frequencies obtained by Fourier analysis (Fourier integral). The frequency response of the integration unit has also to be taken into account. Furthermore, the coils have to be sufficiently sensitive.
These conditions are satisfied reasonably well by the coils of Type I and II. Figures 7 and 8 show the geometries of Type I and II respectively.

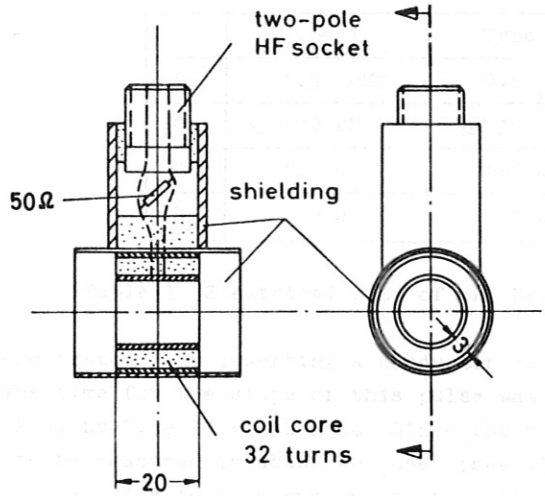

Fig. 7 Rogowski coil type I

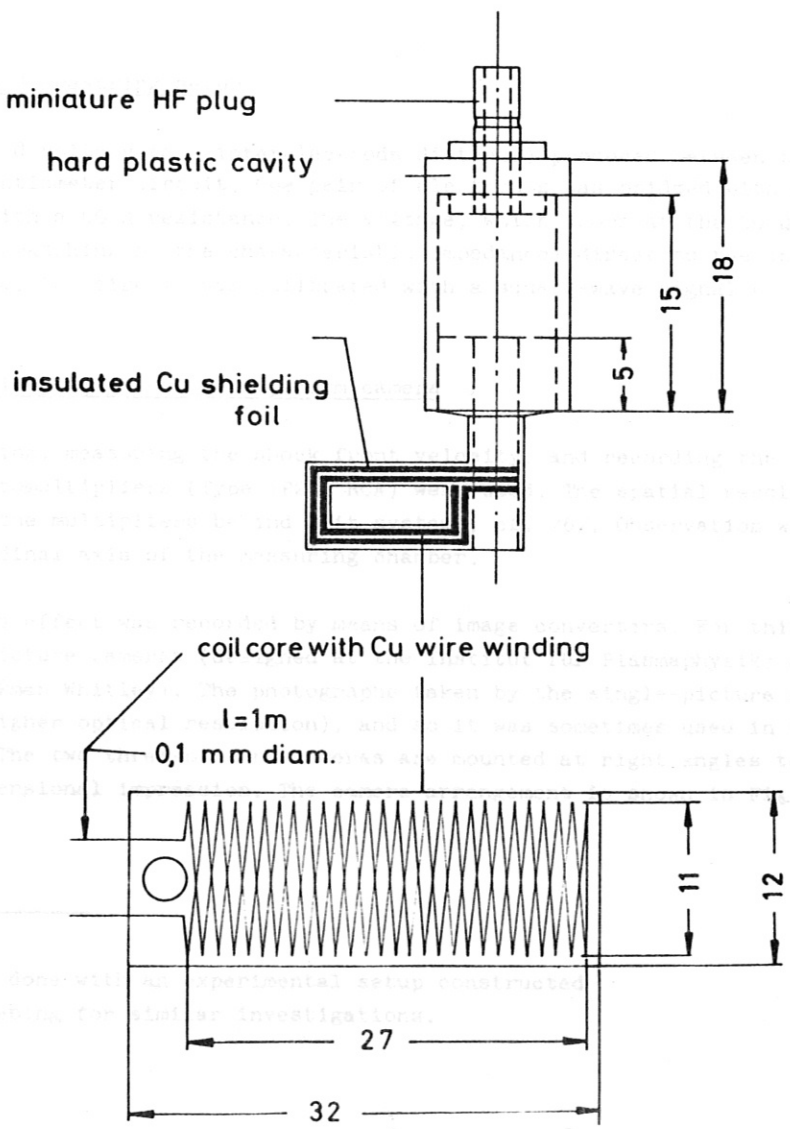

Fig. 8 Rogowski coil type II

The electrical data are listed in Table I, L and R having been measured and C calculated approximately.

	Type I	Type II
L	1.5 µHy	0.5 µHy
C	≈ 100 pF	≈ 30 pF
R	1.8 Ω	1.6 Ω
R_a	50 Ω	50 Ω

Table I Electrical data of the Rogowski coils

Both types of coil were tested[+)] by inserting a conductor in the coil and passing a pulse current through it. The time for the slope of this pulse was 20 nsec. This was distorted by Type I to about 100 nsec, by Type II to 30 nsec. Since the minimum time for the slope (cf. /4/) of the pulse current to be measured is about 20 µsec (see also the oscillograms in Fig. 10), the time resolution of the coils is good enough for the intended purpose.

After electronic integration the sensitivity is:

Type I : 158 mV/kA

Type II : 46 mV/kA

3.2 v · B · d measuring setup

The v · B · d voltage (d = interelectrode distance) produced between two electrodes was measured with a potentiometer circuit. One pair of electrodes was bridged with a 100 kΩ resistance series connected with a 50 Ω resistance. The voltage, which drops at the 50 Ω resistance, was fed by a 50 Ω cable (matching of the characteristic impedance) direct to the input of an ungrounded oscilloscope. The circuit was calibrated with a square-wave signal of known voltage.

3.3 Multiplier, image converter, drum camera

For triggering, measuring the shock front velocity, and recording the luminous effect in the plasma, photomultipliers (Type 1P21, RCA) were used. The spatial resolution was improved by installing the multipliers behind slit systems, cf. /6/. Observation was made on a level with the longitudinal axis of the measuring chamber.

The luminous effect was recorded by means of image converters. For this purpose there were two three-picture cameras (designed at the Institut für Plasmaphysik) and a single-picture camera (Beckman Whitley). The photographs taken by the single-picture camera are slightly superior (higher optical resolution), and so it was sometimes used in conjunction with the other two. The two three-picture cameras are mounted at right angles to one another to convey a three-dimensional impression. The camera arrangement is shown in Fig. 9.

[+)] This was done with an experimental setup constructed by L. Liebing for similar investigations.

The effects due to interaction were recorded with a drum camera (Model 316, Beckman Whitley). For the streak pictures a 5 mm wide slit running the entire length of the measuring chamber was stopped down and imaged on the film (see Fig. 1).
The triggering, recording, and screening operations and the problems entailed are described at length in /4/.

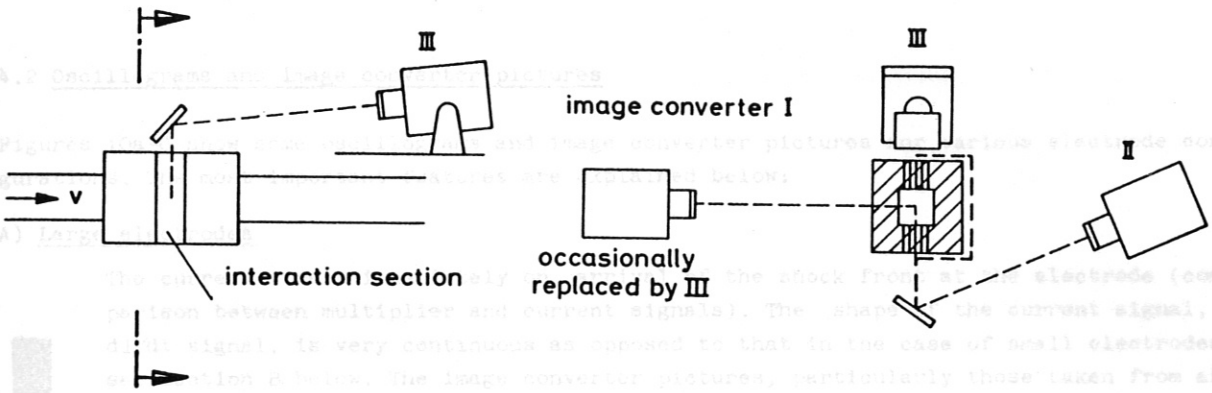

Fig. 9 Arrangement of the image converters. Camera III is the one-picture camera.

4. MEASURING RESULTS AND DISCUSSION

4.1 Measuring procedure

Image converter pictures or streak pictures were made simultaneously with the current measurements. In the case of the image converter pictures the monitor pulses were recorded as well. Each time several multiplier signals of the incandescence were also recorded in order to determine, for example, the coincidence between the arrival of the shock wave at the interaction region and the other observations and to measure the shock front velocity in front of and behind the interaction region. In addition, the time variation of the crowbar signal, i.e. of the magnetic field, was also recorded. The initial pressure p_o and magnetic field B_o were seldom varied.

4.2 Oscillograms and image converter pictures

Figures 10a-d show some oscillograms and image converter pictures for various electrode configurations. The most important features are explained below:

A) Large electrodes

The current starts immediately on arrival of the shock front at the electrode (comparison between multiplier and current signals). The shape of the current signal, see dI/dt signal, is very continuous as opposed to that in the case of small electrodes, see section B below. The image converter pictures, particularly those taken from above, show how arcs strike at several points (indicated by a higher degree of incandescence). These pictures clearly suggest a non-uniform current distribution. The side-on pictures show at first more incandescence near the electrodes, i.e. where the arcs strike. It is only later that the gas becomes more incandescent over the entire cross section of the measuring chamber.

B) Small electrodes

a)
The current starts in the relaxation region and the current amplitude is lower. The image converter pictures also show the shock front (only in the first set of measurements using a new plexiglass section in the measuring chamber) and the plasma boundary, defining in this way the relaxation region. The side-on photograph clearly shows the strong incandescence near the electrodes, i.e. where the arcs strike in the relaxation region. (The window frame causes a shadow in each of these pictures, Fig. 2.) The pictures taken from above also show where the arcs strike in the relaxation region.

b) and c)
At later times as well, the image converter pictures show strong incandescence mainly near the electrodes. On passing through the narrow current channels leading to the electrodes, the gas is excited to strong incandescence. After the gas has passed through them, this incandescence takes some time to disappear. This makes the gas dynamic boundary layer visible c).

d) and e)
If the plasma incandescence occurring without current is appreciably stopped down, the pictures taken at later times show, in the centre of the measuring chamber as well, somewhat stronger incandescence which decays in the flow direction d). If the initial pressure p_o is lower and the incandescence is stopped down even more, it is again possible to observe the boundary layer e). (The pictures taken from above show diffuse incandescence. This is due to the fact that vaporized electrode material is deposited on the walls, thus impairing transparency.)

f) and g)
At the beginning of the measuring series it sometimes happened that the current started very late, e.g. not until shortly before the arrival of the contact front f) or between the shock and contact fronts. This is due to impurities in the form of very thin films on the electrode surfaces, see Section 4.4.3.

h)
The reproducibility of the starting time of the current and the time behaviour of the current was rather good later, as the dI/dt signals of five shots show. The image converter picture obtained from ten shots in which the plasma incandescence (occurring without current) is strongly stopped down shows again incandescence caused by the current near the electrodes and makes the boundary layers visible.

i)
Image converter pictures at p_o = 20 torr without magnetic field also convey a three-dimensional impression of the contact front.

C) Section with 5 electrode pairs, short-circuited 1 pair at a time

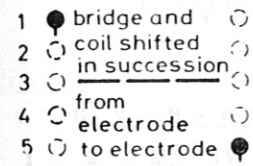

When only one electrode pair is shorted, the current has the same time behaviour, irrespective of the location of the electrodes.

D) 5 electrode pairs transverse to flow direction

a)
The current flows through all five electrode pairs, has the same time behaviour, and can generally be reproduced well. It starts in the relaxation region. The time at which the individual arcs start are different.

b)
Very seldom does the current fail to start at one electrode pair. (The remaining signal is caused by the crowbar discharge.)

c)
Failure of the current to start or delay in starting can also be observed in the image converter pictures taken from below. In side-on observation, the gas becomes incandescent over the entire cross section of the measuring chamber, there being a slight bulge in the flow direction.

E) 10 electrode pairs

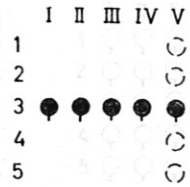

The time behaviour of the current flow is more irregular, see dI/dt signal. The image converter pictures again show where the arcs strike and how the incandescence increases over the entire cross section (there being a slight image distortion due to overexposure of the image converter cathode).

F) 25 electrode pairs

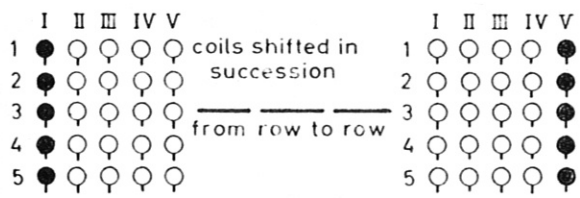

In this case, there are only five coils or integrators available for measuring the current. The rows of electrodes were therefore provided in turn with coils, and several shots were made for each configuration to check the reproducibility. The image converter pictures show whether the arcs strike, and so it can be checked whether current has flowed through all 25 electrode pairs.

Two examples are shown:

a) 1st row of electrodes with coils

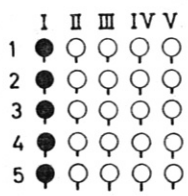

The time behaviour of the current is very irregular and the current amplitude is lower. The perturbations from the crowbar discharge are much larger than those affecting the coil signals in the preceding examples. The times at which the individual arcs start are different. Some do not start until the current maximum of the others is reached. The image converter pictures taken from below show again the striking of the arcs. They are striking at

different times. The side-on picture shows strong incandescence over the entire cross section, there being a slight bulge in the flow direction. (The plasma incandescence occurring without current was stopped down.) This picture suggests a rather uniform current density distribution.

b) 4th row of electrodes provided with coils

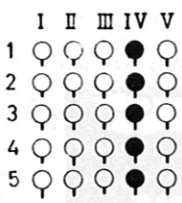

The starting times of the currents are here nearly the same. The current amplitudes, current variations, and perturbations caused by the crowbar discharge are very similar for all rows. The image converter picture taken from below again shows the striking of the arcs. The 3rd picture shows where they are disrupted in the contact front, see monitor signals. In side-on observation, there is again strong incandescence in the entire cross section and bulging in the flow direction.

G) v · B · d measurements

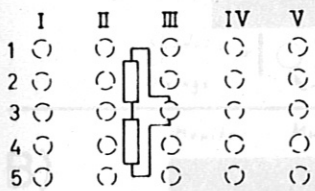

The v · B · d signal is superposed on the dI/dt signal from the crowbar discharge. In the shock front it makes an upward jump and is of approximately rectangular form. This jump coincides with the arrival time of the shock front at the measuring electrode. A small presignal and a small starting-current peak are observed.

H) Bridges in various directions

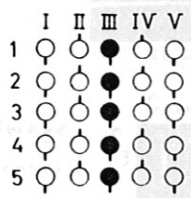

If the bridges of the individual rows alternately face in the opposite direction, the signals from the crowbar discharge are much smaller and the current signal is recognized more readily. An oscillogram shows crowbar signals on the Rogowski coils without plasma flow. The side-on image converter pictures show reproducible incandescence in the entire cross section with bulging in the flow direction (also two shadows caused by the bridges on two rows).

I) Multiplier oscillograms. Observation in front of and behind the interaction region. 25 electrode pairs. Currents as in F)

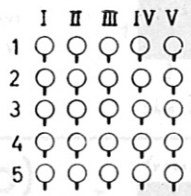

The multiplier oscillograms in front of the interaction region show the usual behaviour, cf. /6/. The shock front, relaxation region, and contact front can be recognized. Behind the interaction region there appear in the relaxation region secondary "peaks", from which it can be concluded that there are many secondary fronts present. At high pressures these fronts are more pronounced.

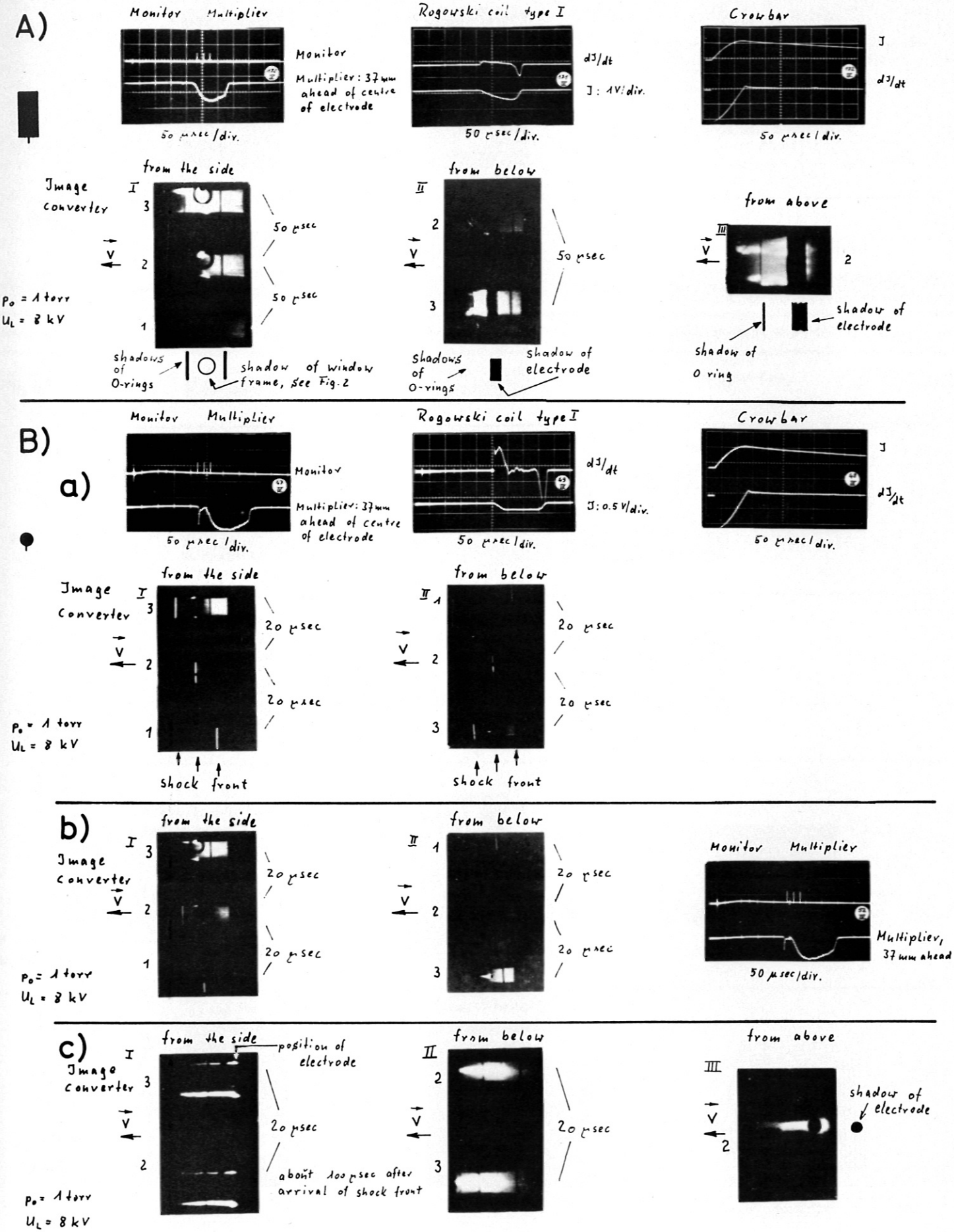

Fig. 10 a Oscillograms and image converter pictures

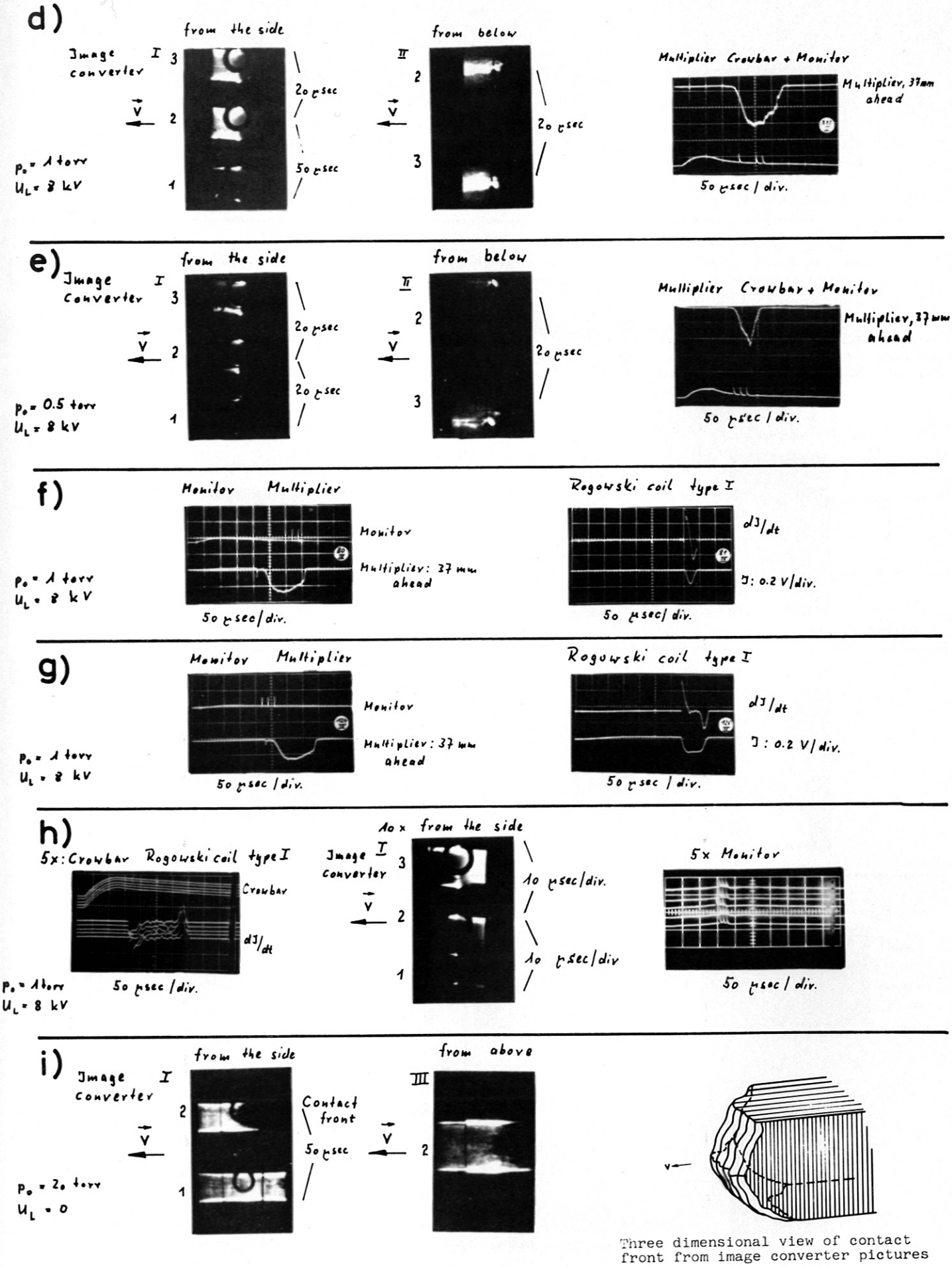

Fig. 10 b Oscillograms and image converter pictures

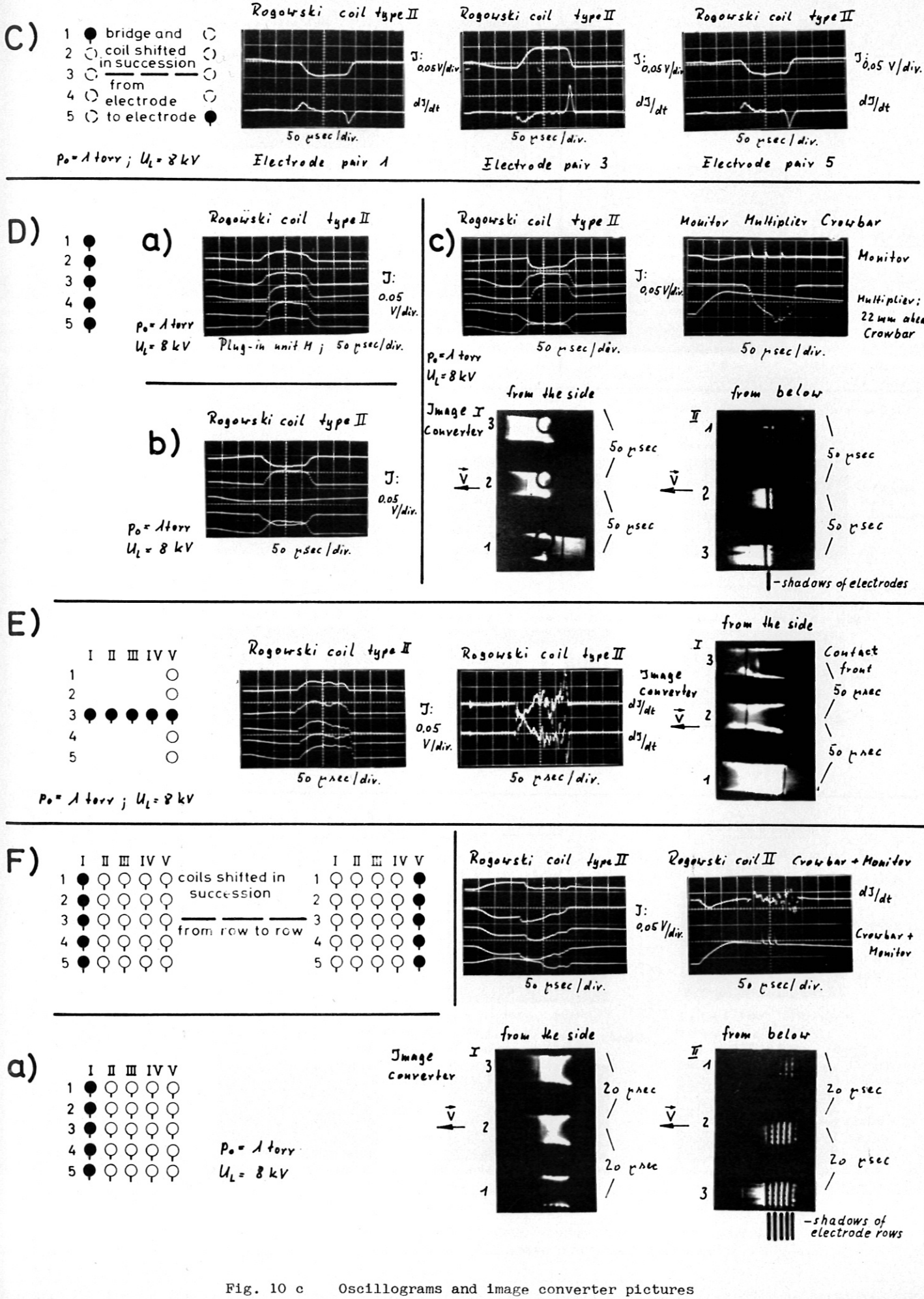

Fig. 10 c Oscillograms and image converter pictures

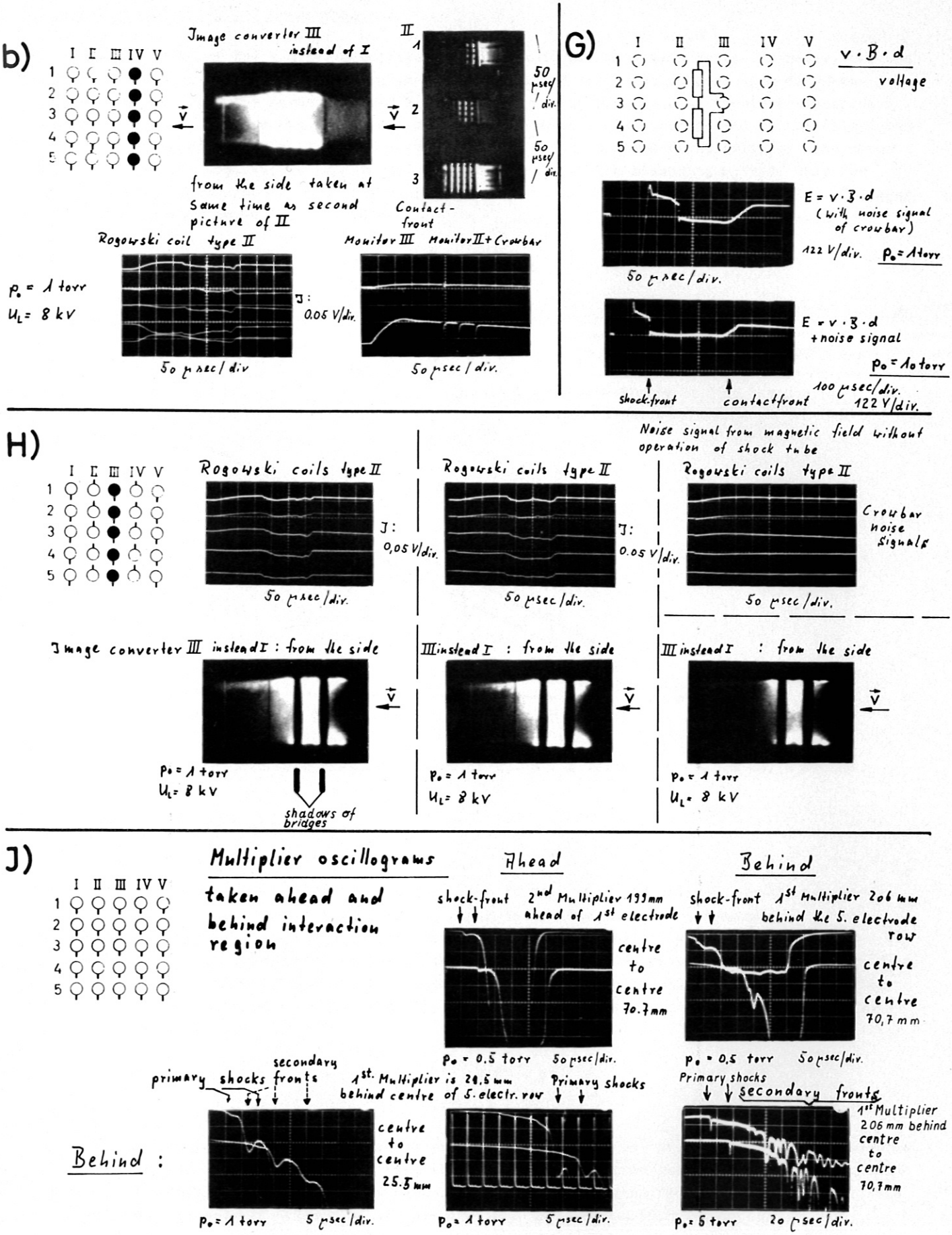

Fig. 10 d Oscillograms and image converter pictures

4.3 Results of v · B · d measurements

The maximum value of the v · B · d voltage can be calculated. This is possible, firstly, because the shock Mach number is known, and so the flow velocity $\vec{v}$ can be calculated with allowance for ionization, cf. /6/. The magnetic field $\vec{B}_o$ is also known, see Fig. 5. d is the interelectrode distance. Figure 11 shows the calculated and measured values. The error spread of the calculated values is governed essentially by the accuracy of the measured shock front velocity. The error spread of the measured values is governed by the accuracy of the measuring method. Only for p_o = 1 torr do the error spreads of the measured and calculated values fail to overlap. The mean deviation (dashed curve) is only 15 %.

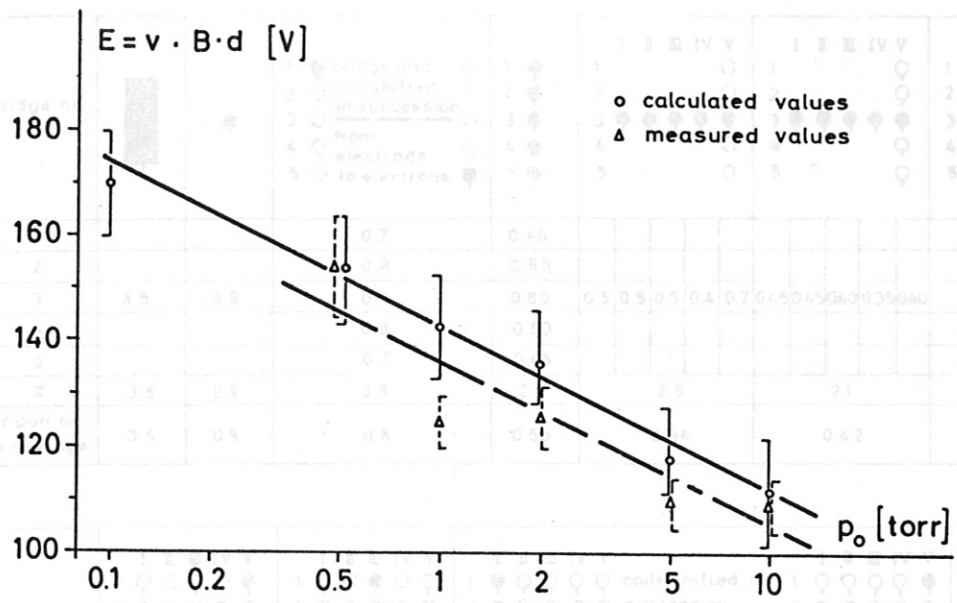

Fig. 11 Calculated and measured values of v · B · d voltage. B_o = 6.8 kG, d = 7 cm.

4.4 Results of current measurements

4.4.1 Evaluation method

When the current varies smoothly (see oscillograms in Fig. 10), the maximum current may serve as a criterion for calculating the retarding $\vec{j} \times \vec{B}$ force. The current behaviour was, however, very irregular, particularly with 25 short-circuited electrode pairs, and the signal of the crowbar discharge was superposed on it. In this case, the integral mean values with respect to time of the pulse current I seem to be a better criterion for calculating the retarding force. These values were therefore formed from all oscillograms showing the current by using a planimeter:

$$I = \frac{1}{t_2 - t_1} \int_{t_1}^{t_2} I(t) \cdot dt$$

where t_1 denotes the time at which the arc strikes (just behind the shock front) and t_2 the time of disrpution (in the contact front). Here the spurious signal from the crowbar discharge, which is recorded separately for each set of measurements, was subtracted from the total signal. This integral mean value is 25 % lower on the average than the maximum value.

4.4.2 Measuring results

Table II shows in kA the arithmetic mean values of these evaluations of many current measurements, i.e. of the integral mean values. The mean error of the individual integral mean values is 15 to 20 %, and the mean error of the mean integral mean value is 2 to 5 %. The mean value of the integral mean current per electrode pair of small surface area decreases with the number of electrodes. This is almost irrespective of whether the electrode pair (in the case of one pair) is located in the centre or at the boundary of the chamber, or whether the electrode pairs (in the case of five pairs, for example) are transverse or parallel to the flow direction. The direction of the bridges here does not have any noticeable influence on the current value, nor does the distance between the short-circuited electrode pairs. This decrease with the number of electrodes is illustrated in Fig. 12.

bridge no.			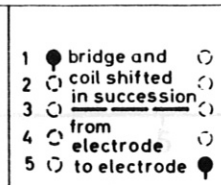	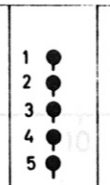	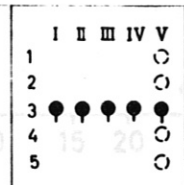	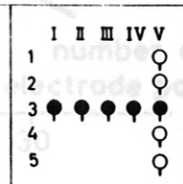	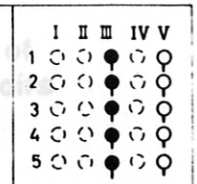
1			0.7	0.45			0.44
2			0.8	0.65			0.50
3	3.5	0.9	0.9	0.60	0.5 0.5 0.5 0.4 0.7	0.45 0.45 0.40 0.35 0.40	0.51
4			0.8	0.50			0.60
5			0.7	0.45			0.52
Σ	3.5	0.9	3.9	2.7	2.6	2.1	2.6
per pair on the average	3.5	0.9	0.8	0.55	0.54	0.42	0.52

bridge no.		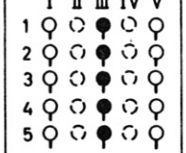	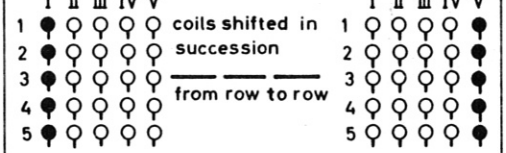	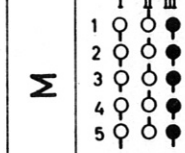	Σ	
1	0.39	0.34	0.24	0.25 0.23 0.20 0.37	1.29	0.19
2	0.38	0.41	0.30	0.30 0.29 0.23 0.33	1.45	0.29
3	0.35	0.30	0.34	0.28 0.20 0.19 0.27	1.28	0.24
4	0.39	0.46	0.31	0.17 0.26 0.15 0.24	1.13	0.16
5	0.44	0.39	0.24	0.21 0.24 0.17 0.28	1.14	0.21
Σ		1.90	1.43	1.21 1.22 0.94 1.49	6.29	1.09
per pair on the average	0.39	0.38	0.25			

Table II

Results of current measurements. Arithmetic mean values of integral mean value with respect to time of the current in kA. Initial pressure p_o = 1 torr. B_o = 6.8 kG.
The mean error of integral mean values is 15 to 20 %. The mean error of the mean values of the integral mean values 2 to 5 %.

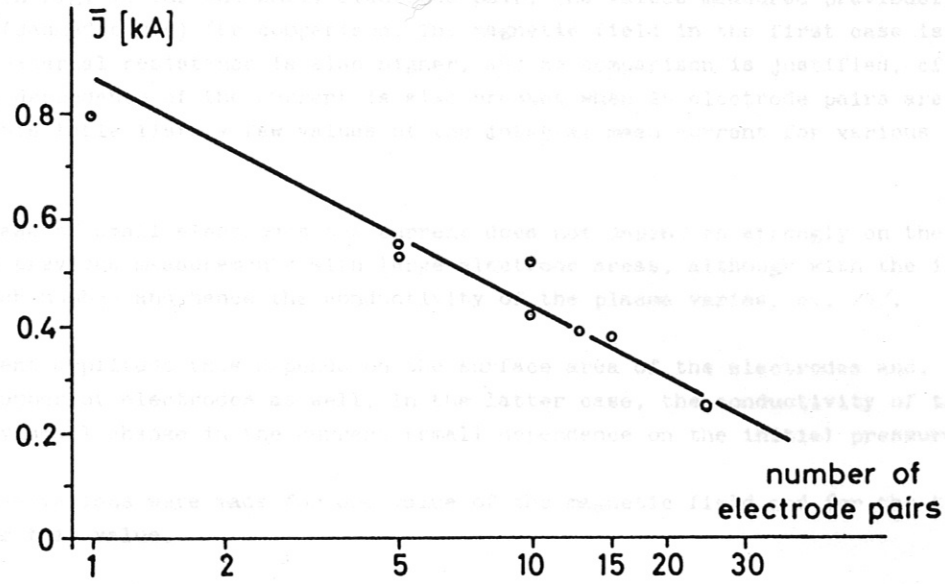

Fig. 12 Arithmetic mean value of integral mean values with respect to time of current per electrode pair vs. number of electrode pairs, see Table II.

The current flowing through the large electrodes is much higher. This variation of the current amplitude with the surface area of the electrodes has been observed before /4/. This dependence is shown for the individual electrode pairs in Fig. 13, in which values measured previously are also included and in which the maximum current is plotted. Above a certain surface area, the current amplitude in the range of surface areas considered here does not vary any more.

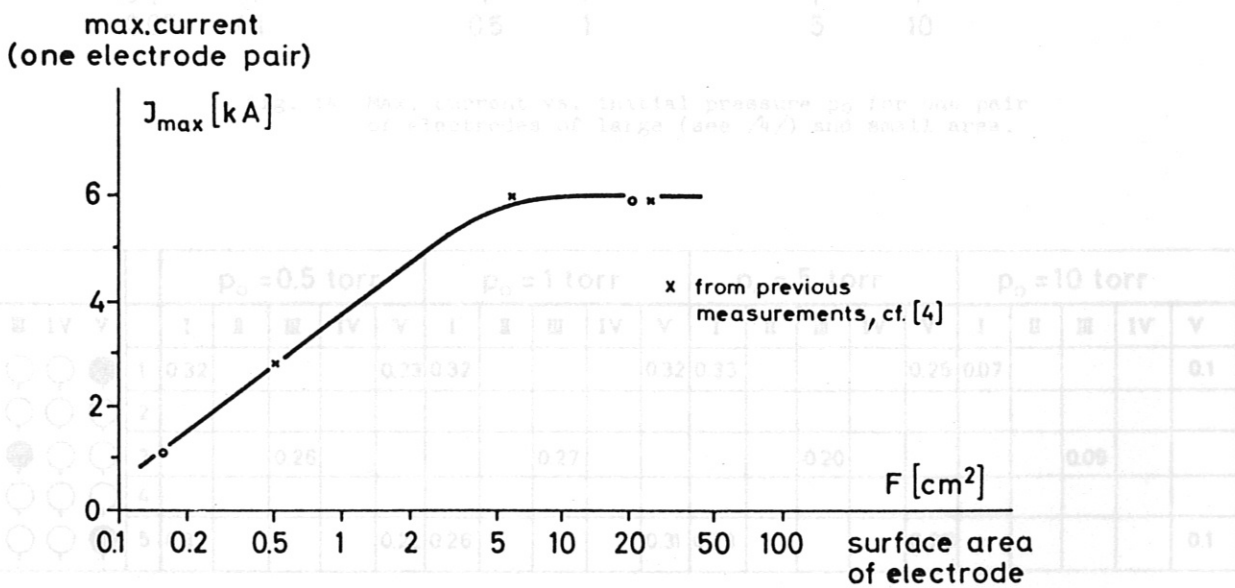

Fig. 13 Max. current vs. surface area of electrode (one electrode pair)

There is a dependence of the maximum current amplitude on the initial pressure p_o which is plotted in Fig. 14 for one small electrode pair. The values measured previously are also plotted (dashed curve) for comparison. The magnetic field in the first case is a little higher, but the external resistance is also higher, and so comparison is justified, cf. /4/. This small pressure dependence of the current is also present when 25 electrode pairs are used, as Table III shows. This table lists a few values of the integral mean current for various initial pressures p_o.

In the case of small electrodes the current does not depend so strongly on the initial pressure p_o as in previous measurements with large electrode areas, although with the initial pressure the shock Mach number and hence the conductivity of the plasma varies, cf. /4/.

The current amplitude thus depends on the surface area of the electrodes and, for small areas, on the number of electrodes as well. In the latter case, the conductivity of the plasma can vary with only small change in the current (small dependence on the initial pressure p_o).

These observations were made for one value of the magnetic field and for the time being are only valid for this value.

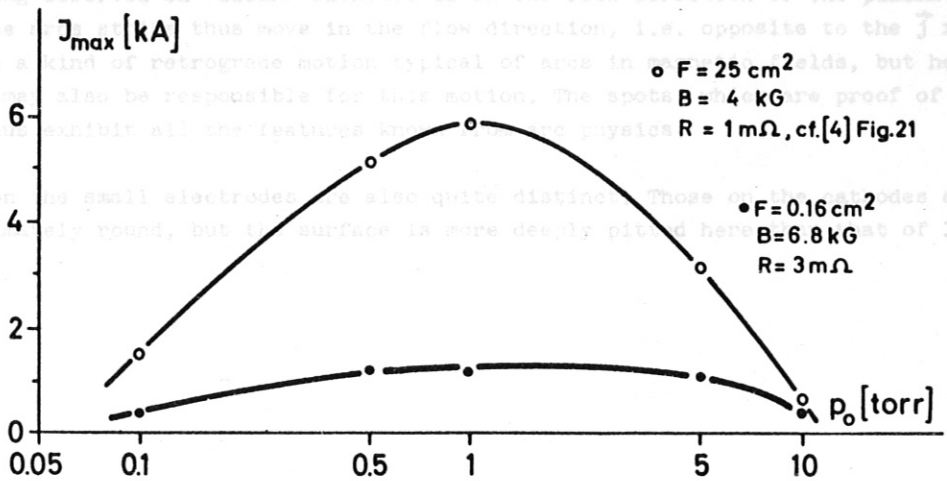

Fig. 14 Max. current vs. initial pressure p_o for one pair of electrodes of large (see /4/) and small area.

		p_o = 0.5 torr					p_o = 1 torr					p_o = 5 torr					p_o = 10 torr				
I II III IV V		I	II	III	IV	V	I	II	III	IV	V	I	II	III	IV	V	I	II	III	IV	V
● ○ ○ ○ ●	1	0.32				0.23	0.32				0.32	0.33				0.25	0.07				0.1
○ ○ ○ ○ ○	2																				
○ ○ ● ○ ○	3			0.26					0.27					0.20					0.09		
○ ○ ○ ○ ○	4																				
● ○ ○ ○ ●	5	0.37				0.22	0.26				0.31	0.33				0.28	-				0.1

Table III

Arithmetic mean values of integral mean values of current in kA. Variation of initial pressure p_o, B_o = 6.8 kG.

4.4.3 Arc spots

The existence of arc spots on large electrodes has already been pointed out in previous investigations /4/, but it has not been the subject of any detailed discussion. Figure 15a-d shows pictures of spots that appeared on the cathodes and anodes in these investigations, cf. Fig. 27 in /4/. Such spots were also observed in the investigations described here, these being shown in Fig. 15e for the case of small electrodes (case E in Fig. 10c).

On the anodes there appear small round spots that are spread over the entire surface (Fig. 15a, b,c). The spots on the cathodes (Fig. 15b,c) are irregular in shape. The arc spots move along and also across the grooves caused by machining. If the surface is chemically and mechanically cleaned (the simplest mechanical method being to let gas behind the shock wave pass without a magnetic field, i.e. without current), there are then no arc spots on the anodes and those on the cathodes change shape (Fig. 15d). Many traces that look like Lichtenberg figures can then be seen branching out in the flow direction $\vec{v}$ (right-hand side), these being longer in the flow direction than in the direction of the grooves.

The round spots on the anodes are thus due to thin layers of impurities. This phenomenon has also been observed in ordinary arcs without magnetic field and transverse flow /10/.

The branching observed on "clean" cathodes is in the flow direction of the plasma. The points at which the arcs strike thus move in the flow direction, i.e. opposite to the $\vec{j} \times \vec{B}$ force. This may be a kind of retrograde motion typical of arcs in magnetic fields, but here the supersonic flow may also be responsible for this motion. The spots, which are proof of the existence of arcs, thus exhibit all the features known from arc physics.

The spots on the small electrodes are also quite distinct. Those on the cathodes are smaller and approximately round, but the surface is more deeply pitted here than that of large electrodes.

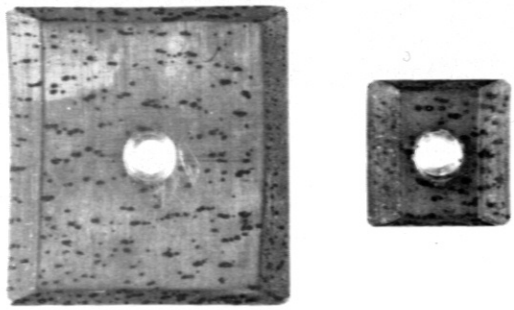

a)

Copper anodes of different areas after many shots

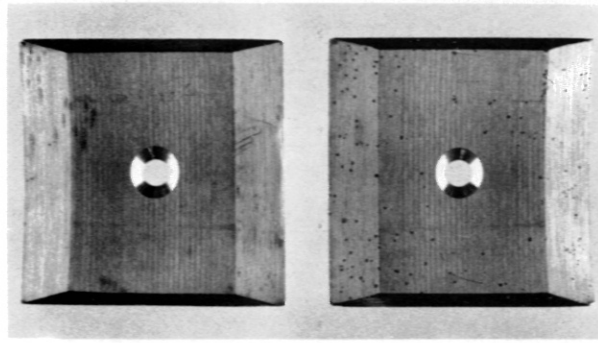

Cathode b) Anode

5 x 5 cm^2, brass, after <u>one</u> shot

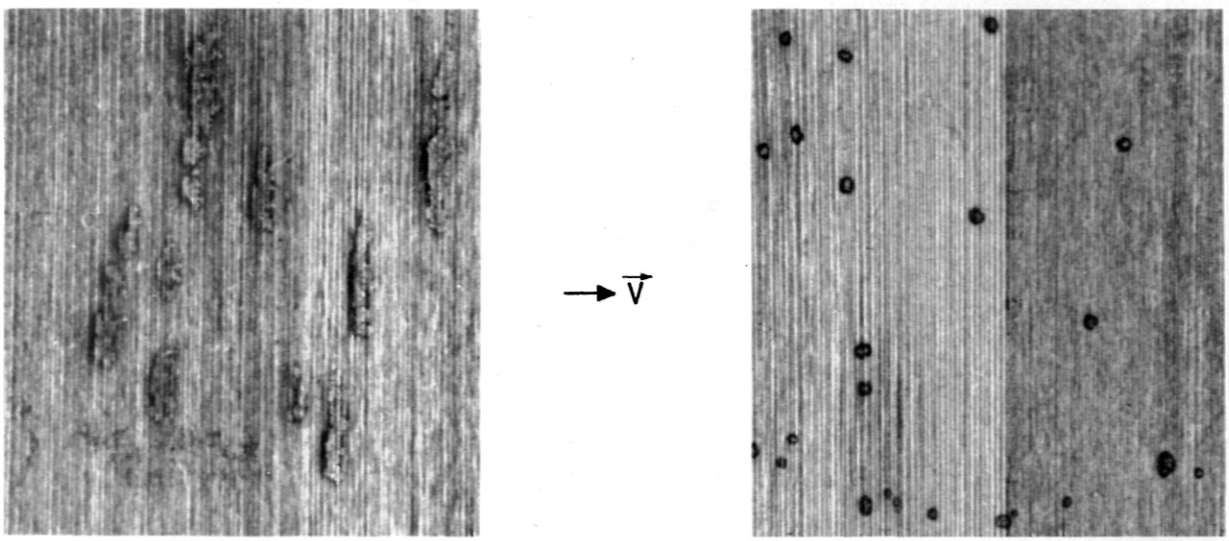

Cathode c) Anode

Enlarged sections of b) (see Fig. 26 in /4/)

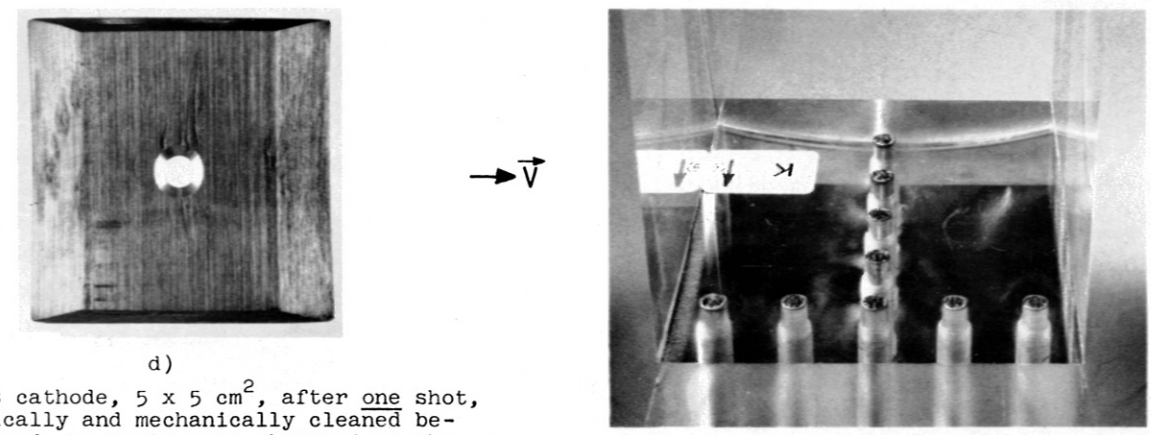

d)

Brass cathode, 5 x 5 cm^2, after <u>one</u> shot, chemically and mechanically cleaned beforehand. No spots were observed on the corresponding, likewise cleaned anode.

e)

Cathodes of 4.5 mm in diam., after many shots

Fig. 15 Spots on anodes and cathodes, see /4/.

4.5 Internal resistance of the current channel

4.5.1 One electrode pair

The simple equivalent circuit diagram in Fig. 16 can be used in this case (cf. /4/).

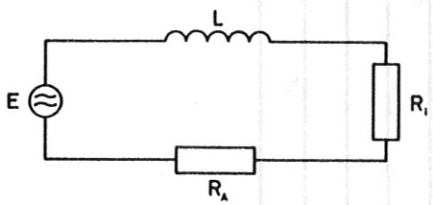

Fig. 16 Equivalent circuit diagram of pulse generator (see Fig. 2 in /4/).

L = total inductance of the discharge circuit (short-circuiting bridges with electrodes and current channel in plasma)

R_i = total internal resistance (current channel)

R_a = total external resistance (electrodes and short-circuiting bridges)

E = generator emf

$E(t) = v \cdot B \cdot d \cdot s(t)$

d = effective interelectrode distance

s(t) = time dependent factor (max. amplitude = 1) that describes the time behaviour of the emf and that is known from measurements, see oscillograms in Fig. 10d. This curve is almost rectangular.

The inductance can be assumed constant, and R_a as well. R_i depends on the current I and hence on the time. On these assumptions it holds that

$$E(t) = L \cdot \frac{dI}{dt}(t) + R_i(I(t)) \cdot I(t) + R_a \cdot I(t)$$

Since L, R_a, E(t), I(t), and dI/dt(t) are known from the measurements, the time behaviour of the internal resistance can be determined, cf. /4/. In order to estimate a mean value of R_i, let us consider the centre of the current pulse, for which dI/dt is very small and can be neglected:

$$R_i = \frac{E_{max} - R_a \cdot I_{max}}{I_{max}}$$

For an external resistance of 3 mΩ, see Section 2.4, a value of

$$R_i \approx 25 \text{ m}\Omega$$

is obtained for the large electrode and a value of

$$R_i \approx 140 \text{ m}\Omega$$

for the small electrode if the flow velocity v originally due to the shock Mach number is taken as a basis at a pressure of p_o = 1 torr. (The retarding force can reduce the velocity, and then the value of E decreases, and hence that of R_i as well. But this can be neglected in the case of one electrode pair.)

4.5.2 5 electrode pairs

When five electrode pairs transverse to the flow direction are used (in which case the shock front reaches all electrodes at the same time and the voltage E is therefore produced at the same time), it begins to become more difficult to design an equivalent circuit diagram because the short-circuiting bridges are close together and the single circuits are inductively coupled to a high degree. The equivalent circuit diagram in Fig. 17, in which only the inductive coupling is taken into account, is taken as a basis for estimating the internal resistance per circuit. M_{12} is the mutual inductance between the circuits 1 and 2.

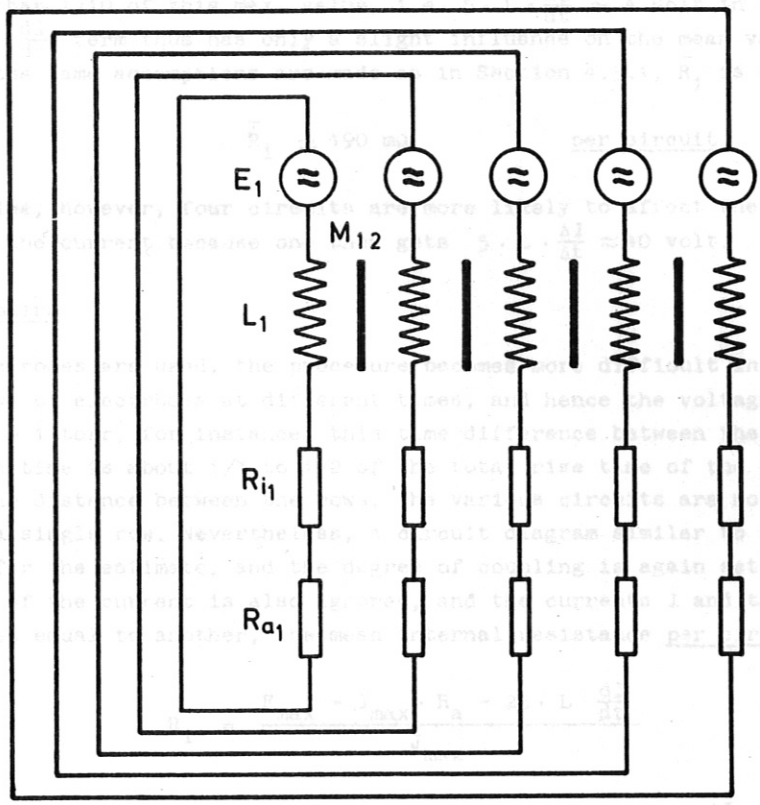

Fig. 17 Equivalent circuit diagram of 5 inductively coupled circuits

The inductive coupling factor of the circuits can be set approximately equal to unity because the individual magnetic fluxes almost completely penetrate the current loops, see Fig. 2. The self-inductances of the individual circuits do differ slightly, see Section 2.4, but they can all be approximated by the mean value 0.4 μHy. Similarly, the mean value 3 mΩ can be used for the external resistances. The values of E are the same for all circuits. Because of the assumption that the coupling factor is equal to unity, all mutual inductances can be set approximately equal to the mean self-inductance. The following system of equations is then valid:

$$E = I_1 (R_a + R_{i1}) + L \frac{dI_1}{dt} + \frac{dI_2}{dt} + \text{---} + \frac{dI_5}{dt}$$

$$\vdots$$

$$E = I_5 (R_a + R_{i5}) + L \frac{dI_1}{dt} + \qquad\qquad + \frac{dI_5}{dt}$$

Apart from R_i, all parameters are again known from previous measurements, and the system of equations can be solved for R_i.

For further estimates one can set $I_1 \approx I_2 \approx \text{- - -} \approx I_5$ and $\frac{dI_1}{dt} \approx \frac{dI_2}{dt} \approx \text{- - -} \approx \frac{dI_5}{dt}$. The mean internal resistance per circuit is then:

$$\bar{R}_i = \frac{E_{max} - I_{max} \cdot R_a - 5 \cdot L \cdot \frac{dI}{dt}}{J_{max}}$$

In the centre of the current pulse, the remaining dI/dt is less than 1/10 of the max. value in the slope, see oscillograms in Fig. 10. This max. value dI/dt in the slope can be approximated as $\Delta I/\Delta t$ of the slope from the oscillograms. It is found to be $2 \cdot 10^7$, i.e. $L \cdot \frac{\Delta I}{\Delta t} = 8$ volts. The term $L \cdot \frac{dI}{dt}$ is less than 1/10 of this max. value, i.e. $5 \cdot L \cdot \frac{dI}{dt} \approx 4$ volt in the centre of the current pulse. The $L \cdot \frac{dI}{dt}$ term thus has only a slight influence on the mean value of the internal resistance, and, if the same assumptions are made as in Section 4.5.1, $\bar{R}_i$ is found to be

$$\bar{R}_i \approx 190 \text{ m}\Omega \qquad \underline{\text{per circuit}}.$$

During the current rise, however, four circuits are more likely to affect the fifth and influence the starting time of the current because one then gets $5 \cdot L \cdot \frac{\Delta I}{\Delta t} \approx 40$ volt.

4.5.3 25 electrode pairs

When 25 pairs of electrodes are used, the procedure becomes more difficult in that the shock front reaches the rows of electrodes at different times, and hence the voltage E is applied at various times. At p_o = 1 torr, for instance, this time difference between the first and fifth rows is 15 µsec. This time is about 1/3 to 1/2 of the total rise time of the current signal. Moreover, owing to the distance between the rows, the various circuits are no longer so closely coupled as those of a single row. Nevertheless, a circuit diagram similar to that in Fig. 17 is taken as a basis for the estimate, and the degree of coupling is again set equal to unity. If the delayed start of the current is also ignored, and the currents I and the dI/dt (as in Section 4.5.2) are set equal to another, the mean internal resistance per circuit is found to be:

$$R_i = \frac{E_{max} - I_{max} \cdot R_a - 25 \cdot L \frac{dI}{dt}}{J_{max}}$$

dI/dt can again be estimated in the form $\Delta I/\Delta t$ from the oscillograms. $L \cdot \frac{\Delta I}{\Delta t}$ is found to be about 4 volts. In the centre of the current pulse the dI/dt is about 1/10 of this value, i.e. $\frac{25}{10} \cdot L \cdot \frac{\Delta I}{dt} \approx 10$ volts. The term $I_{max} \cdot R_a$, on the other hand, is only 0.9 volts, but E is 140 volts for p_o = 1 torr if the flow velocity behind the primary front is taken as a basis. The flow is in fact slowed down, see Section 4.7. The extent to which the flow is slowed down can vary from row to row. If the flow is assumed to slow down to the velocity of sound in the electrode region, a value of about 70 volts is obtained for E. The term describing the inductive coupling then has an influence: it corrects the value of $R_i(t)$ relative to the case of one electrode pair where dI/dt can practically be set equal to zero in the pulse centre. When the slowing down is ignored, the mean internal resistance $\bar{R}_i$ is about

400 mΩ per circuit.

With allowance for the fact that the flow is slowed down to the velocity of sound, the mean internal resistance is still 200 mΩ. During the current rise, the effect of the dI/dt should again be taken into account. 24 circuits can produce in a 25th one a voltage of approximately 100 volt and opposite to E, and so the start may be delayed (as can be seen in Fig. 10).

The change of E due to the magnetic field of the currents (other B) was not taken into account. In approximation, the B_z is reduced by the currents at the beginning of the interaction region and increased at the end. The mean field is again B_o, which was used for the estimate.

The change of the mean value of the internal resistance merely reflects the variation of the current with, for example, the number of electrode pairs. The inductive coupling can affect essentially only the start and the rise time of the current.

4.6 Discussion of the results

The total internal resistance is composed of the internal resistance of the current channel in the plasma flow and that of the plasma-to-electrode transition. In all of the cases discussed, the conductivity of the plasma, which is governed by the shock Mach number, is very high, e.g. σ_1 = 40 mhos for p_o = 1 torr. On the assumption that the conductivity of the plasma is not changed very much by the current, it is then possible to use the value of the internal resistance to calculate what volume is required to produce this internal resistance in the plasma, cf. /4/. The radius of a cylindrical discharge column is found from $F = \pi r^2 = d/\sigma_1 R_1$, e.g. for the case of 25 electrode pairs, to be r = 3.7 mm, whereas the distance between the rows of electrodes is 14 mm. The available volume is thus much larger. Therefore it follows that most of the internal resistance is formed by the plasma-to-electrode transition and not by the plasma itself. This transition consists of the narrow arc channels leading to the arc spots and the arc spots themselves.

The pictures of the arc spots demonstrate that the arcs in this case are of the type with non-stationary spots, described in the literature, e.g. /11/. In such arcs, numerous small spots appear and disappear continually on the cathode. The current densities in the spots are very high (up to 10^6 A/cm^2). There are probably both ions and electrons carrying the current. The ions streaming to the cathode then produce in front of it the high field that makes electron emission possible. The energy input due to the impact of ions causes the temperature of the cathode spot to rise until the energy lost as a result of thermal conduction and vaporization of the material is equal to the energy input. The ions emanate from the high temperature plasma layer in front of the cathode. This plasma layer is heated by the electrons, which come from the cathode and are accelerated in the cathode fall region, and by the neutralized positive ions reflected as neutral atoms from the cathode. The layer maintains its high temperature because the conduction of energy to the cathode remains small owing to contraction of the layer. This contraction causes the forming of the current channels in front of the spots. In the region of the arc spot, the cathode surface is so loosely packed to a depth of several atomic layers, this state being due to the high energy transferred by ion collisions, that it is difficult to say whether this state is that of a highly disturbed solid or of a highly compressed plasma.

Despite numerous investigations, the transition phenomena in such arcs have not yet been explained quantitatively because the conditions are extremely complex. (Even thin layers of impurities can have an influence, as the measurements show.) The phenomenon of retrograde motion, which was probably observed in our case as well, is prominent among the transition phenomena not yet explained satisfactorily.

Since our case is even more complicated, viz. with transverse magnetic field and supersonic flow, there seems to be no hope of explaining our results quantitatively. The phenomena observed can, however, be understood qualitatively by comparing them with those described in the literature on normal arcs. Such a comparison seems reasonable because many of the properties observed here agree with those of normal arcs.

1. In order to check the dependence of the current on the electrode surface area below a certain size, let us study the pictures of the arc spots (Fig. 15). In the case of large electrodes there are many arc spots at some distance from one another.
The current amplitude must be governed by the number of spots. On the other hand, a certain distance is expected between the spots, i.e. between the current channels, owing to the space charge density distribution and hence to the potential distribution in front of the cathode.
In the case of small electrodes there is no such minimum distance, and the number of arc spots, and hence the current amplitude, should become smaller.

2. The decrease of the current amplitude with the number of electrode pairs can be explained by the mutual influence of the space charges in front of the electrodes. This affects the formation of spots, the number of which governs the current amplitude.

3. The small influence of the initial pressure p_o, i.e. the conductivity of the streaming plasma, on the current amplitude in the case of small electrodes, is due to the fact that the current amplitude is governed essentially by the boundary conditions. In the case of large electrodes, the arc spots together provide so much current that the internal resistance of the transition becomes comparable with that of the streaming plasma. The conductivity of the plasma then becomes effective.

4. The time variation of the current (dI/dt) in the centre of the current pulse is smallest for one pair of large electrodes and largest for 25 pairs of small electrodes. This is because there are so many arc spots on large surfaces that the effect of their migration, disappearance, and appearance is averaged out in time, approximately at least. In the case of small surfaces, however, the effect may become more pronounced, especially when 25 electrode pairs are involved, because the potential distribution is of a very complicated nature owing to the mutual influence of the current channels. Moreover, the slowing down of the plasma flow may have an effect in the latter case.

5. Occasional failure of the current to start or delay in starting, see Fig. 10, can be explained in terms of the influence of impurities deposited on the electrodes.

The total current that can be drawn using many small electrodes is not much higher than that for large electrodes, but the current distribution is certainly much more uniform.

4.7 Calculation of the retarding force $\vec{j} \times \vec{B}_o \cdot L$

The real aim here is to fill the interaction volume with current as uniformly as possible. The image converter pictures suggest that this has been achieved. There is, however, a certain amount of bulging in the flow direction, this being possibly due to relaxation. The current density distribution is not known, of course, but it seems reasonable to assume that it is uniform in the electrode region. On this assumption, it is possible to calculate roughly the retarding force acting on the flow: With 25 electrode pairs present, the total integral mean current is $I \approx 6.25$ kA for initial pressures of 0.5 to 5 torr and $I \approx 2.5$ kA for $p_o = 10$ torr. The distance between the electrode pairs is 1.4 cm. If it is assumed that the interaction volume is uniformly filled with current and that the current flows perpendicularly to v, the mean interaction length is $L \approx 7$ cm and the mean cross-sectional area of the current is $F \approx 7 \times 7$ cm^2. The mean current density is then:

$$j = \frac{J}{F} \approx 127 \frac{A}{cm^2} \quad \text{and} \quad j \approx 51 \frac{A}{cm^2} \quad \text{respectively.}$$

This can be used together with the external magnetic field to calculate the retarding force P_x per unit area, which is:

$$P_x = j \cdot B_o \cdot L \approx 6 \cdot 10^5 \text{ dyne/cm}^2 \text{ and } 2.4 \cdot 10^5 \text{ dyne/cm}^2 \text{ respectively.}$$

The total hydrodynamic pressure of the unperturbed flow is:

$$p_1 + \rho_1 \cdot v_1^2$$

and this can be calculated, cf. /4/. Table IV shows the calculated values of the ratio of the retarding force to the total hydrodynamic pressure for various initial pressures. The table also includes the magnetic Reynolds number. The results indicate that, if the assumptions made are valid, the retarding force should have a noticeable effect, at least at low initial pressures, because the retarding force is of the order of the total hydrodynamic pressure.

p_o torr	$\frac{j \cdot B_o \cdot L}{p_1 + \rho_1 \cdot v_1^2}$	$R_m = \frac{\mu_o \cdot j \cdot L}{B_o}$
0.5	0.7	0.18
1	0.5	
2	0.3	
5	0.2	
10	0.04	0.07

Table IV

Calculated values of the ratio of the retarding force $j \cdot B_o \cdot L$ to the total hydrodynamic pressure of the flow and the magnetic Reynolds number. 25 electrodes. B_o = 6.8 kG.

Using more electrodes in the flow direction will elongate the interaction length L, but on the other hand the total current will decrease, see Fig. 12. Doubling this length by using, for example, 50 pairs of small electrodes would give a total current of 7 kA if one could extrapolate from Fig. 12. This value of the total current is nearly the same as in the case of 25 pairs. The mean cross-sectional area would be about twice the value, and the current density half the value, i.e. the retarding force would be about the same value as with 25 electrode pairs. Using more electrodes will therefore not produce an appreciably stronger retarding force.

Using only five electrode pairs transverse to the flow direction would shorten the interaction length L by a factor of perhaps four (taking into account a changed distribution of current). The total current would be smaller by a factor of about 2 (see Table II), the cross-sectional area by a factor of about 4, and the current density would then be twice the value, but the retarding force only about half the value compared with the case of 25 electrode pairs. Furthermore, in this case of five electrode pairs the current distribution would be more inhomogeneous in the flow direction.

Another possibility is the use of a smaller number of electrodes with larger surface area. This would again influence the current distribution.

Choosing 25 pairs of electrodes seems to be a reasonable compromise.

4.8 Results of drum camera measurements

4.8.1 Streak pictures

Figure 18 shows some streak pictures taken over the entire length of the measuring chamber. The initial pressure p_o is taken as parameter. B_o is 6.8 kG. Number of electrode pairs is 25. At p_o = 0.1 torr, the plasma slab between shock and contact fronts is not long enough to allow interaction effects to be clearly recognized. It can be seen, however, that the plasma flow is deflected in the interaction region.

At p_o = 0.5 torr, the plasma flow makes a sharp bend in the interaction region, thus indicating a decrease of velocity. There is another front which runs counter to the flow until it reaches the contact front and is reflected from it in the downstream direction, finally catching up with the primary front. These fronts can be recognized more clearly in the colour photograph in Fig. 19.

At p_o = 1 torr, the reflected front becomes more obvious, the bend in the flow less so. Secondary fronts can be observed behind the primary front. These were also detected with multipliers, cf. Fig. 10d.

With increasing pressure above p_o = 2 torr, the velocity of the reflected front decreases until it comes to rest in the flow and is finally carried along by it. The number of secondary fronts increases with the initial pressure, see the multiplier pictures in Fig. 10d.

All streak pictures show the velocities of the reflected fronts to be time dependent.

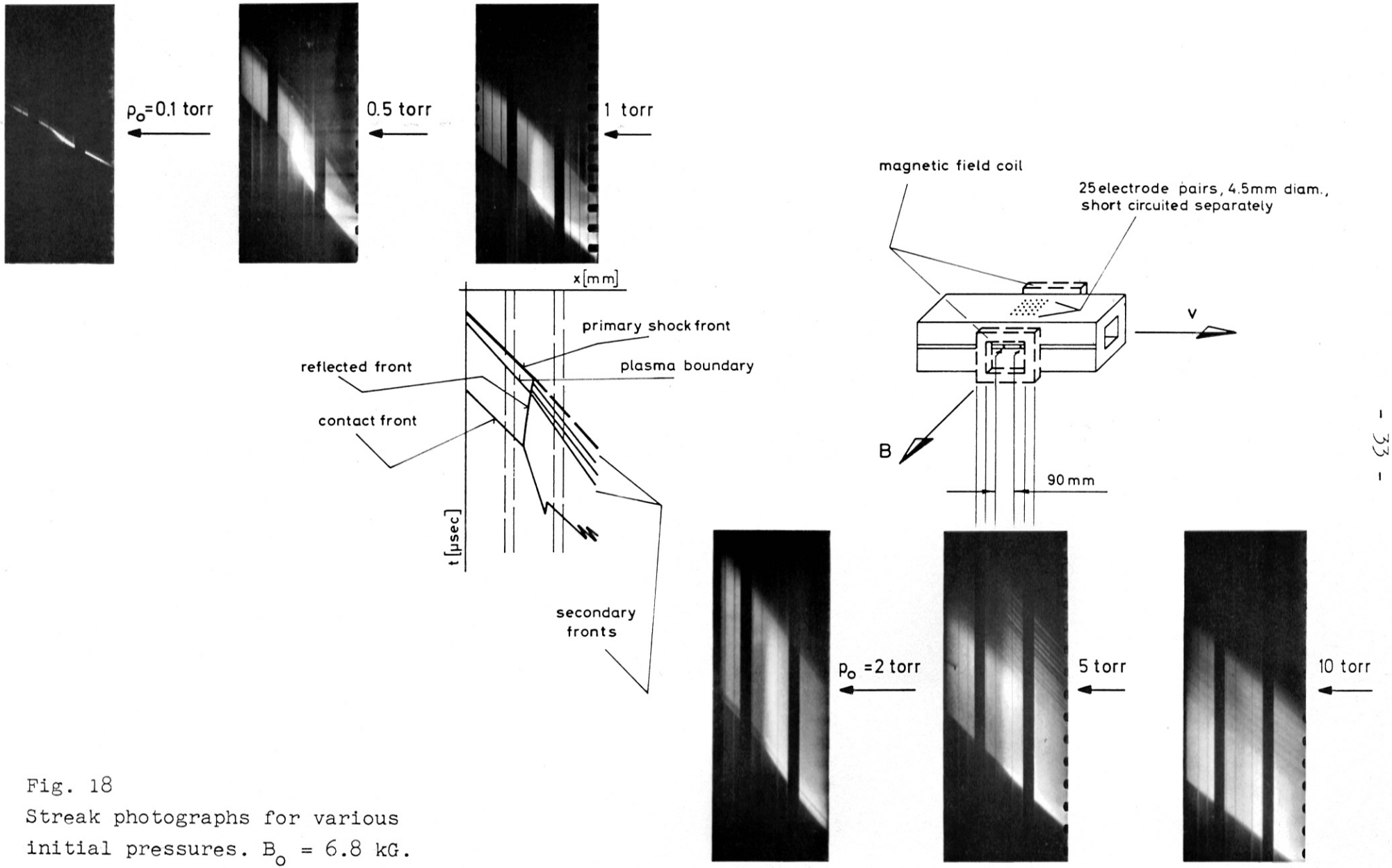

Fig. 18
Streak photographs for various initial pressures. B_o = 6.8 kG.

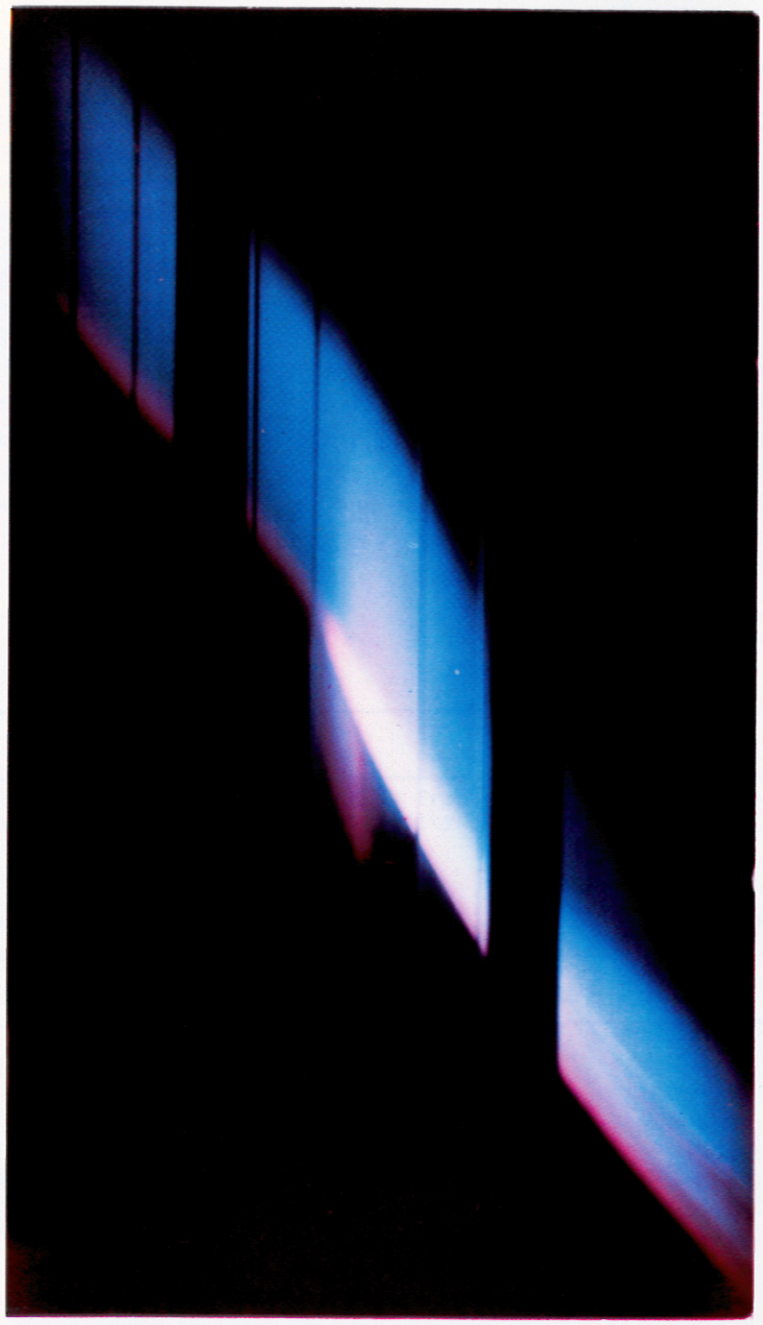

Fig. 19 Streak picture
p_o = 0.5 torr, see Fig. 18

4.8.2 Velocity of the observed fronts

A device for differentiating curves was used to evaluate the streak pictures with respect to the velocity of the reflected fronts. The results are shown in Fig. 20, cf. Fig. 18. The direction of the flow velocity $\vec{v}$ behind the primary shock front is taken as positive. The relative values refer to the calculated flow velocity $\vec{v}$ which the plasma has behind the unperturbed primary shock front. The arrows indicate the development with time. At low initial pressures p_o, the velocities of the reflected fronts decrease to the flow velocity $\vec{v}_1$. At high initial pressures p_o, the front is swept along by the flow (reversal of direction). Figure 21 shows the velocity of the front, which is again reflected at the contact front for p_o = 0.5 torr. This front leaves the interaction region and its velocity increases in the downstream direction.

Behind the primary shock front one can observe secondary fronts which are the stronger the higher the initial pressure p_o. The velocity of the first secondary front at p_o = 1 torr is, for example, 2.7 ± 0.2 mm/µsec.

4.9 Results of the multiplier measurements

The multiplier measurements yield the velocities U_s or the shock Mach number M_s of the primary shock in front of and behind the interaction region. In addition, the velocity U of the first secondary front behind the primary shock front was determined after it had passed through the interaction region. The shock Mach number can be used to calculate the flow velocity v_1 behind the shock front. The results for p_o = 1 torr are shown in Table V. The shock Mach numbers in front of the interaction region for the other pressures agree within the measuring accuracy with previous results, e.g. /4/. The secondary fronts were observed with the multipliers from two directions that are mutually perpendicular and perpendicular to the shock tube axis.

In front of interaction region			Behind interaction region			
shock front velocity U_s mm/µsec	shock Mach number M_s	flow velocity v_1 +) mm/µsec	shock front velocity U_s mm/µsec	shock Mach number M_s	flow velocity v_1 +) mm/µsec	velocity of secondary front U mm/µsec
3.6 ± 0.1	11.5 ± 0.3	2.9 ± 0.1	3.1 ± 0.1	10 ± 0.3	2.4 ± 0.1	2.7 ± 0.1

+) theoretical

Table V

Results of measurements with photomultipliers. p_o = 1 torr. B_o = 6.8 kG. 25 electrode pairs.

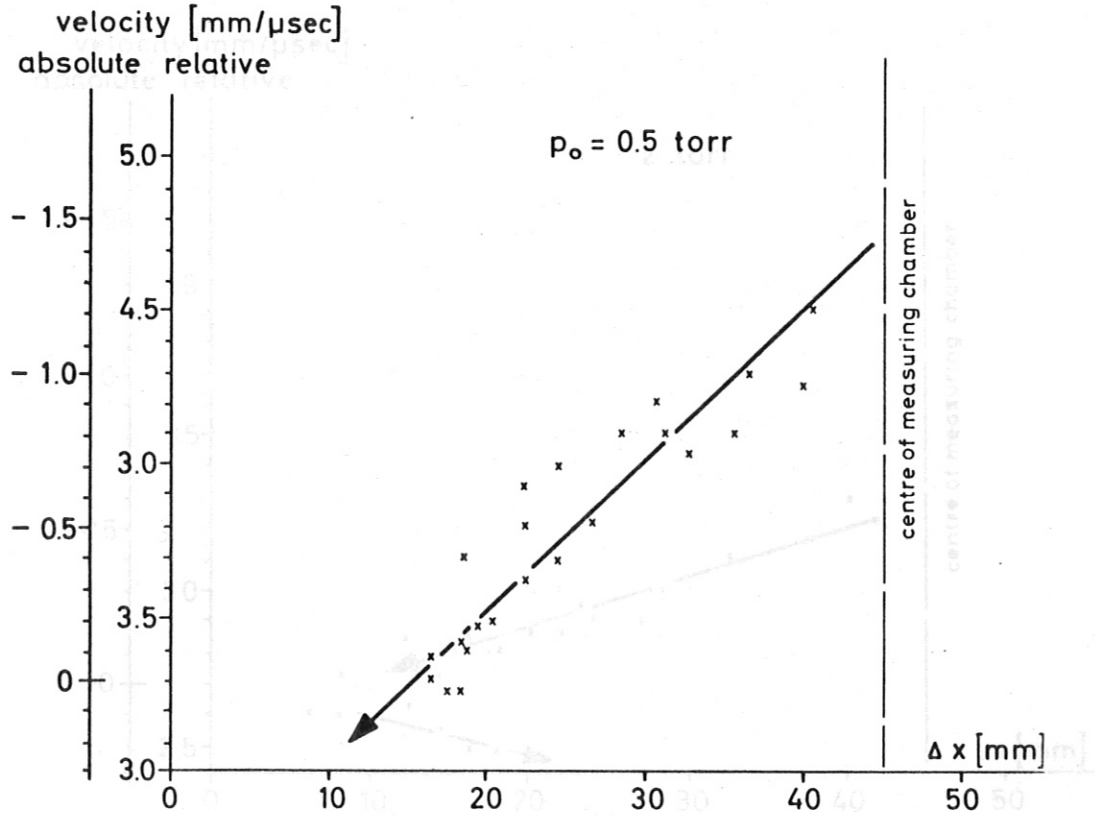

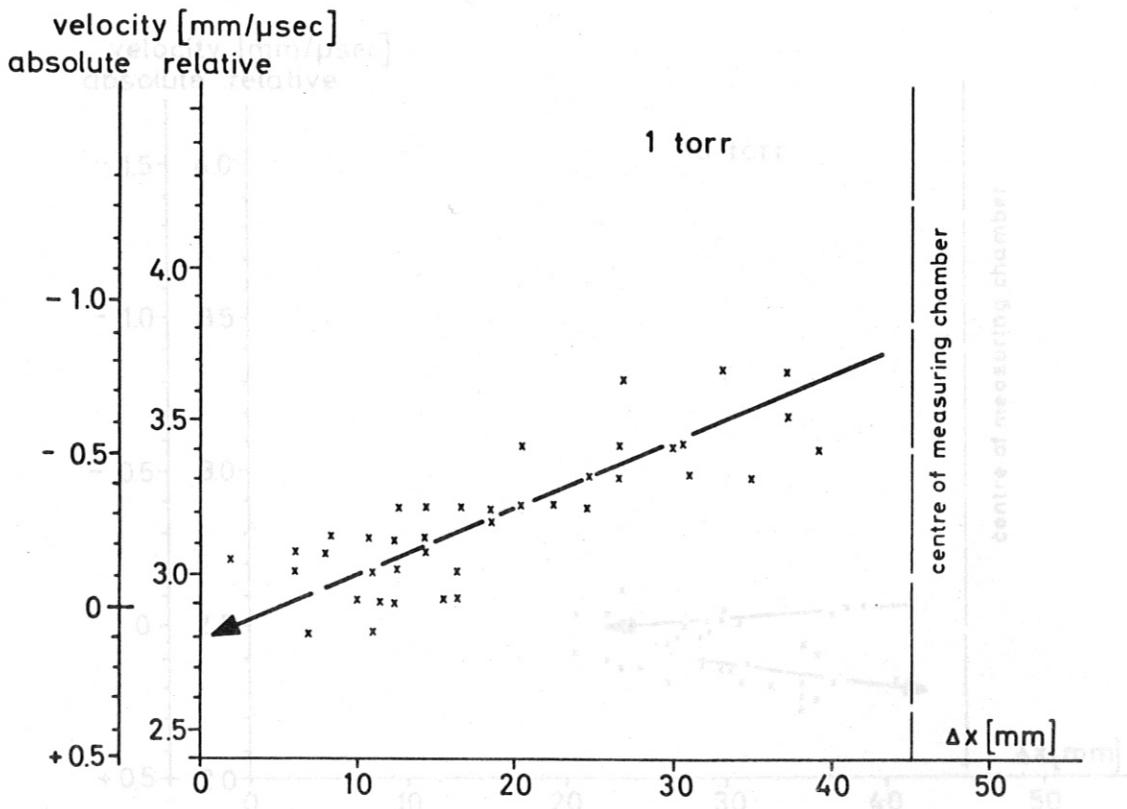

Fig. 20a Velocities of reflected fronts. The relative values refer to the flow velocity. The arrows indicate the development with time.

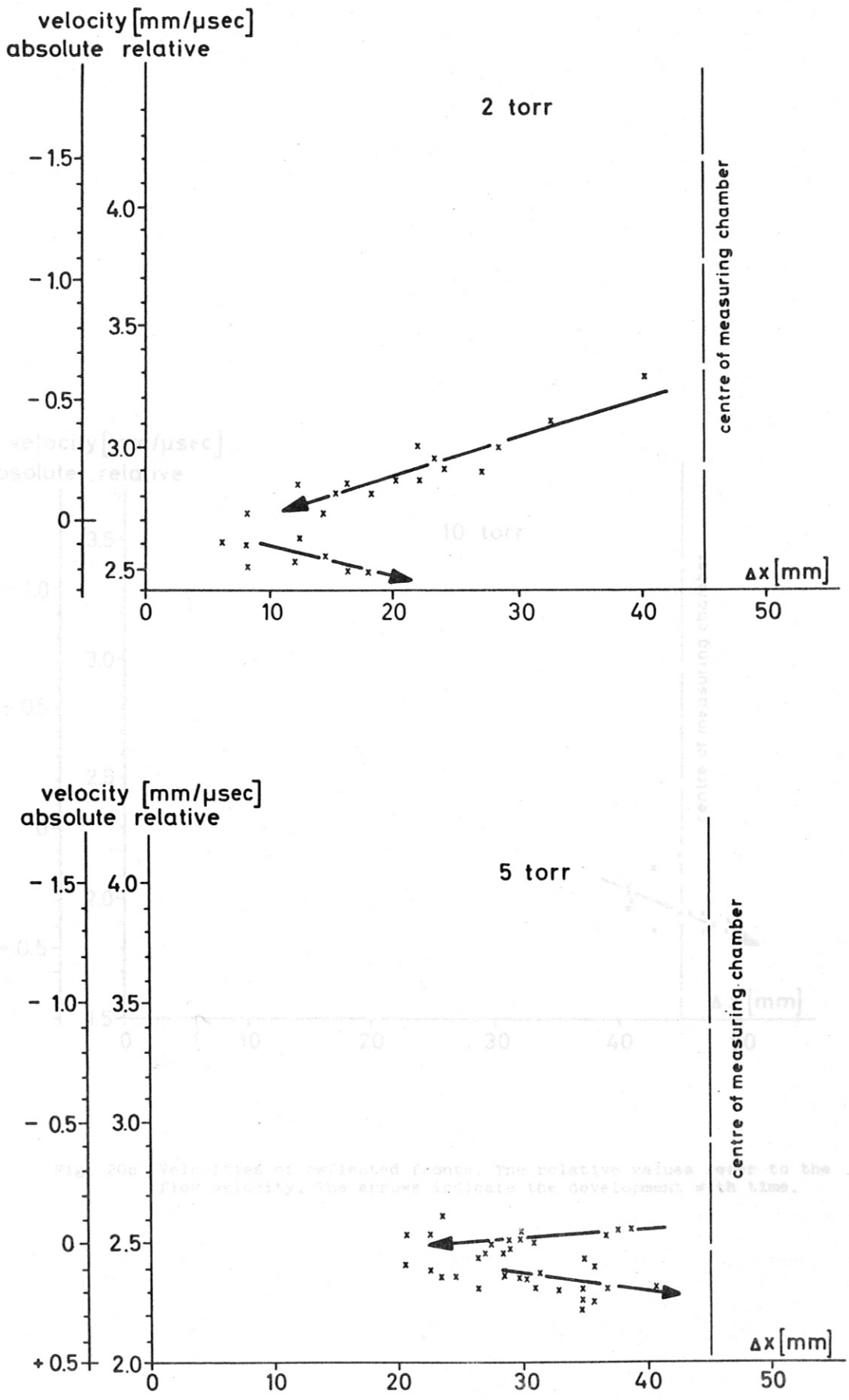

Fig. 20b Velocities of reflected fronts. The relative values refer to the flow velocity. The arrows indicate the development with time.

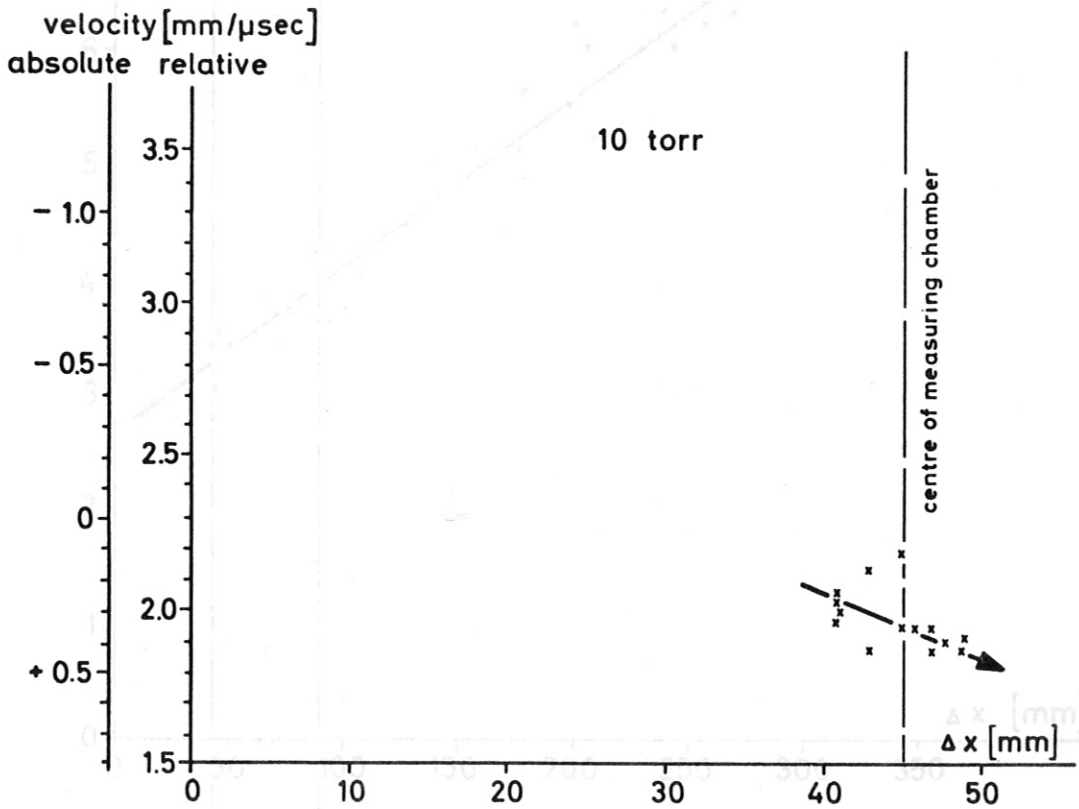

Fig. 20c Velocities of reflected fronts. The relative values refer to the flow velocity. The arrows indicate the development with time.

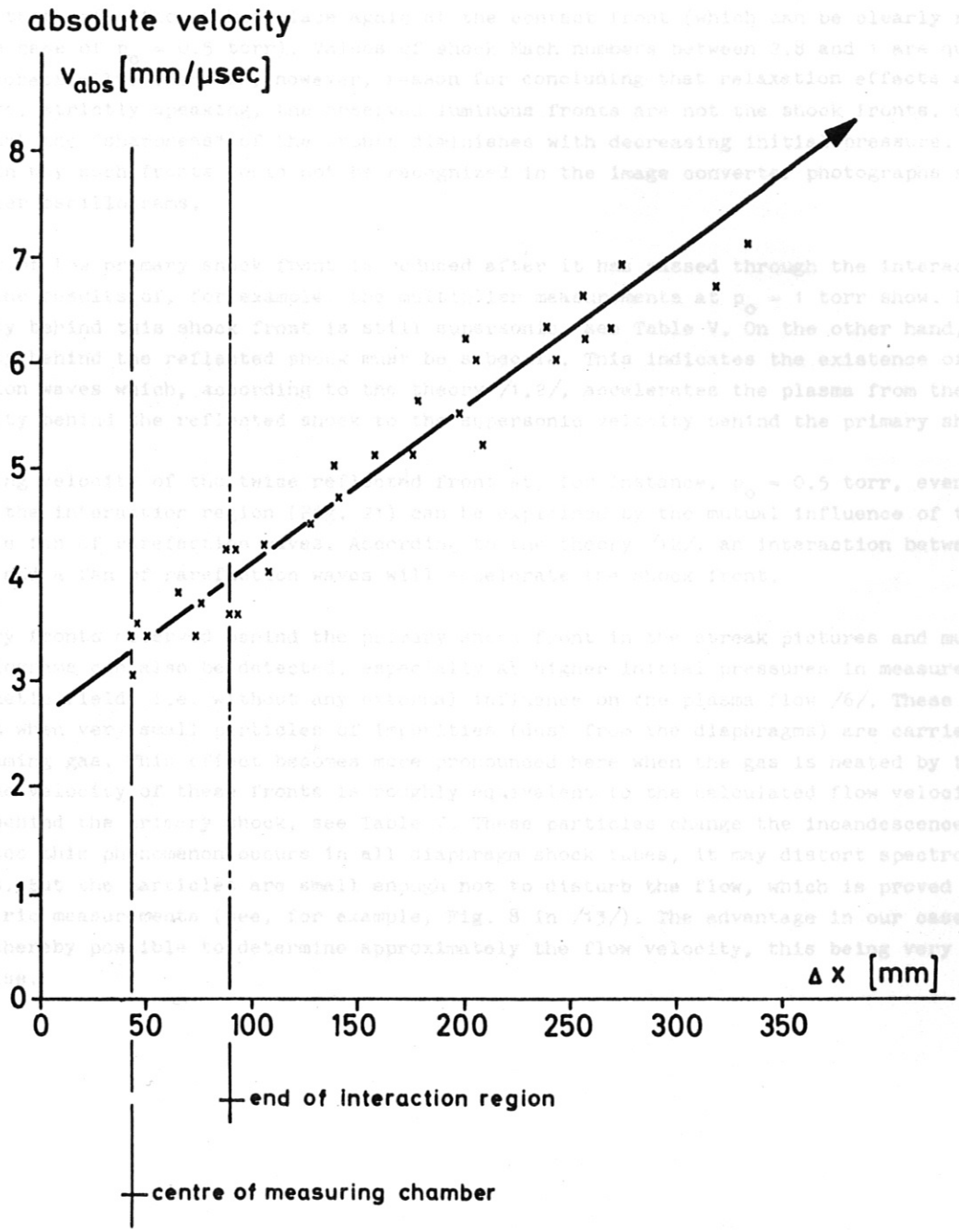

Fig. 21 Velocity of front reflected at contact front for p_o = 0.5 torr

4.10 Discussion of the drum camera and multiplier measurements

As expected from the estimate of the retarding forces (cf. Table IV), the plasma flow is slowed down. The velocity of the reflected fronts decreases with increasing initial pressure. This agrees with the calculated decrease of the retarding force with growing initial pressure. The local velocity of sound in the unperturbed plasma is 1.6 mm/μsec. The reflected fronts observed therefore travel with supersonic velocity relative to the streaming plasma. Their Mach number varies between 2.8 and 1.3, depending on the initial pressure. These are probably shock waves. This is supported by the fact that reflection takes place again at the contact front (which can be clearly recognized in the case of p_o = 0.5 torr). Values of shock Mach numbers between 2.8 and 1 are quite possibly theoretically. There is, however, reason for concluding that relaxation effects are involved and so, strictly speaking, the observed luminous fronts are not the shock fronts. One reason is that the "sharpness" of the fronts diminishes with decreasing initial pressure. This would explain why such fronts could not be recognized in the image converter photographs and in the multiplier oscillograms.

The velocity of the primary shock front is reduced after it has passed through the interaction region, as the results of, for example, the multiplier measurements at p_o = 1 torr show. But the flow velocity behind this shock front is still supersonic, see Table V. On the other hand, the flow velocity behind the reflected shock must be subsonic. This indicates the existence of a fan of rarefaction waves which, according to the theory /1,2/, accelerates the plasma from the subsonic velocity behind the reflected shock to the supersonic velocity behind the primary shock.

The increasing velocity of the twice reflected front at, for instance, p_o = 0.5 torr, even after it has left the interaction region (Fig. 21) can be explained by the mutual influence of this front and the fan of rarefaction waves. According to the theory /12/, an interaction between a shock front and a fan of rarefaction waves will accelerate the shock front.

The secondary fronts observed behind the primary shock front in the streak pictures and multiplier oscillograms can also be detected, especially at higher initial pressures in measurements without magnetic field, i.e. without any external influence on the plasma flow /6/. These fronts are produced when very small particles of impurities (dust from the diaphragms) are carried along by the streaming gas. This effect becomes more pronounced here when the gas is heated by the currents. The velocity of these fronts is roughly equivalent to the calculated flow velocity of the plasma behind the primary shock, see Table V. These particles change the incandescence of the gas. Since this phenomenon occurs in all diaphragm shock tubes, it may distort spectroscopic measurements. But the particles are small enough not to disturb the flow, which is proved by interferometric measurements (see, for example, Fig. 8 in /13/). The advantage in our case is that it is thereby possible to determine approximately the flow velocity, this being very difficult otherwise.

5. CONCLUDING REMARKS

The results of these investigations show that it is possible to utilize the arcs pronounced by $\bar{v} \times \bar{B}$ forces to achieve an approximately uniform current distribution. With this current distribution, gasdynamic effects such as reflected shock waves are produced by $\bar{j} \times \bar{B}$ interaction.

Other investigations, mainly quantitative will be necessary, however, to compare the experimental results with a theory which, though transient is one-dimensional. Mach-Zehnder interferometer measurements, for instance, were begun to prove that the observed fronts are plane shock fronts associated with one-dimensional flow and to detect other gasdynamic effects. In addition, the electron and neutral atom densities behind the fronts are to be measured.

Only then can the experimental results be reasonably compared with the theory. The transient part of the theory of M.R. Johnson /2/ describing effects in the interaction region can be taken as a basis. However, the assumption made in this theory that the current density can be expressed in terms of $\sigma \cdot v \cdot B$ is not valid. The current density here is governed by the complex boundary conditions and cannot be calculated, as is done, for example, in MHD generators at low current densities. The current density has thus to be determined experimentally. Furthermore, ionization effects have to be taken into account.

A theory describing the flow pattern after reflection of the reflected front at the contact front has yet to be formulated.

In further experiments it is hoped to produce reflected shocks leaving the interaction region by increasing the magnetic field, i.e. the retarding force. If then a sort of steady state can be achieved, the theory of Rebhan /1/ can be taken as a basis, allowance again being made for ionization effects.

The difficulties confronting quantitative interpretation of the arc phenomena can only be overcome, if at all, by numerous investigations of the boundary phenomena. This, however, would go beyond the scope of this experiment. No predictions can therefore be made, and so the currents and the current densities have to be measured again for every change of the geometry or of a parameter. It is not known, for example, whether the current becomes larger or smaller with the magnetic field.

REFERENCES

/1/ E. REBHAN, Report IPP 3/28, August (1965)

/2/ M.R. JOHNSON, Phys. Fluids 10, pp. 539-546, (1967)

/3/ H.J. PAIN and P.R. SMY, Brit. J. Appl. Phys. 7, p. 1585, (1966)

/4/ H. KLINGENBERG and H. MUNTENBRUCH, Report IPP 3/45, November (1966)

/5/ H. KLINGENBERG, Contr. Paper of the 8th Int.Conf. on Phen.Ioniz.Gases, Vienna, (1967)

/6/ H. NETT, Report IPP 3/43, October (1966)

/7/ H. OERTEL, Stoßrohre, Springer-Verlag, Vienna-New York, (1966)

/8/ W. ZIMMERMANN, Report IPP 3/57, September (1967)

/9/ F. LABUHN and K. WEINHARDT, Report MPJ - PA - 5/63

/10/ J.M. SOMERVILLE and C.T. GRAINGER, Brit. J. Appl. Phys. 7, p. 109,(1956)

/11/ W. FINKELNBURG and H. MAECKER, Handbuch der Physik, Vol. XXII

/12/ G.A. BIRD, J. Fluid Mech. 15, pp. 282 - 288,(1963)

/13/ H. KLINGENBERG and A. SIDDIQUI, Zeitschrift f. Naturforschg. 23a, p. 752, (1968)